
7

RESIDUAL STRESS IN PIPELINES

PAUL PREVÉY AND DOUGLAS HORNBAUGH

Lambda Technologies, Cincinnati, OH, USA

7.1 INTRODUCTION

This chapter is intended to provide an overview of residual stresses for engineers engaged in the design, installation, and maintenance of pipelines. Residual stresses introduced into pipelines by welding and forming during assembly, installation, or repair and their effect on service life are often overlooked. The goal of this chapter is to provide a general presentation of residual stresses, how they relate to applied stresses, and their influence in service performance of pipelines and related applications. Avoiding creating detrimental tension when possible and dealing with unavoidable tension by thermal stress relief or the introduction of beneficial compression for improved performance are covered. The effects of residual stresses on stress corrosion cracking (SCC) and fatigue failure mechanisms are briefly discussed, but are covered in detail elsewhere in this volume. Practical methods of measuring residual stresses that may be of use to a pipeline engineer are included, with emphasis on their relative advantages and limitations. In addition to the macroscopic residual stresses of primary interest to the engineer, a brief discussion of cold working and “microstress” and their effect upon corrosion behavior is included.

7.1.1 The Nature of Residual Stresses

Residual stresses, sometimes referred to as “self-stresses” or “internal stresses,” are those stresses that are present in a body when it is free of any externally applied forces. Residual stresses are as real as applied stresses, and will generally be retained in a component, such as a section of

welded pipe, assembled coupling, or flange joint for the entire service life. Residual stresses are additive to the applied stresses with which engineers are primarily concerned in the design of a pipeline, and the summation of stress governs performance in service. Tensile residual stresses are generally detrimental, but compressive residual stress can markedly improve performance. The magnitude of residual stresses can often exceed the applied stresses, and can therefore have a major impact on the performance in service.

Residual stresses can be considered to be of two types—macroscopic and microscopic, which are distinguishable by X-ray or neutron diffraction. Macroscopic residual stresses extend over distances that are large relative to the size of the crystals or grains of the material on the order of millimeters. Macroscopic residual stresses are directly additive to the applied stresses, which engineers must consider, due to mechanical loads and pressures on a pipeline. Microstresses are the result of plastic deformation, or cold work, of the metallic material and are very local stresses that extend over distances between the dislocations present within the individual crystals in the metal, on the order of fractions of a micrometer. Microstresses can alter material properties, such as yield strength and corrosion behavior, influencing how the sum of applied and macroscopic residual stresses affect performance.

Although the term “cold working” is sometimes used to imply introducing macroscopic residual compression, as by shot peening (SP) or roller burnishing, it is important to realize that there is no definite relationship between macro- and microstresses, or residual stress and cold work. Stress is a

tensor property, whereas cold work is a scalar property describing the degree of plastic deformation the material has experienced. A body can be uniformly highly cold worked, but nearly stress free. Alternatively, simple bending can produce residual stresses equal to the yield strength with very little cold working. The term residual stress, used here, refers to macroscopic residual stress. Cold work refers to the combination of dislocation density and microstrain causing work hardening.

Residual stresses are caused by nonuniform plastic deformation of either thermal or mechanical origin, or by phase transformations, such as case hardening of steels. Although residual stresses are caused by plastic deformation, regardless of the complex thermal–mechanical history, the residual stresses remaining once the deformation occurred and the body is in equilibrium are necessarily entirely elastic. No matter how complex is the thermal mechanical history of smelting, rolling, forming, grinding, welding, and so on that may have occurred to produce a state of stress, the residual stresses remaining after that complex processing will be entirely elastic. The residual stresses are necessarily limited to less than the yield strength of the material in its then cold-worked or heat-treated condition. The strains due to the elastic residual stresses can then be measured by mechanical dissection or diffraction techniques, and used to calculate the residual stresses present.

7.1.2 Sources of Residual Stresses

Residual stresses encountered in pipelines may arise from a variety of sources, such as the original fabrication of the pipe sections, welding, forming, machining, grinding, handling, and even assembling of the pipeline. The final state of residual stress in any section of pipe will arise from the differences in the amount of plastic and elastic strains created by the combined thermal–mechanical history.

Pipe sections fabricated as rolled, longitudinally welded sections can contain residual stresses from both the forming into the cylindrical shape and the welding of the pipe along the seam [1]. Helical welded pipe will have a more complex stress distribution, again due to the forming and welding. Extruded pipe, although seamless, may have a through-wall stress distribution created in the piercing and drawing operations [2].

Any bending of pipe to form curved sections will necessarily produce tensile residual stresses on the inside of the bend (intrados), which is driven into compression during bending, and compressive residual stresses on the outside (extrados) of the bend, which is stretched in tension. The highest tensile residual stresses are often encountered at the point of tangency just entering into the bend on the inside surface, because the highest plastic strain gradient during bending is at the beginning of the bend. Flaring or other sizing of pipe or tubing to alter diameter will produce residual stresses that can be in high tension at the point of

transition into the increased diameter. Any process that nonuniformly deforms a metal component will result in residual stresses, potentially up to the yield strength of the material. Tensile stresses will be produced in the areas that are plastically deformed in compression during the forming operation; compressive stresses will occur in the regions deformed in tension.

The residual stress distribution in any body must be in equilibrium after external forces and tractions are removed. Equilibrium requires that the sum of the moments and forces acting on any plane entirely through the body must be zero. Equilibrium does not imply that there should be equal and opposite residual tension and compression in adjacent locations in a component. For example, a layer of equal magnitude tension does not occur immediately beneath the compressive layer produced by shot peening a section of pipe. Low-magnitude tension extending through the thick wall will balance the thin compressive layer. A region of residual tension may exist through the entire thickness of a component, such as a pipe wall that has been heated locally so that it is deformed in compression by thermal expansion entirely through the wall, and then cooled. The zone of through-thickness tension is supported in equilibrium by surrounding material in lower magnitude compression.

Welding to join pipe sections is a primary source of residual stress [3]. Welding creates regions that are heated to a liquid or highly plastic state, fused, and then allowed to cool locally. The contraction of the metal upon cooling stretches the fusion zone into high tension, typically up to the yield strength. A zone of residual tension then extends out into the heat-affected zone (HAZ) on either side of the weld [4]. The complex distribution of residual stress, with regions of high tension in a 304 stainless steel T-weld, is shown as a contour plot in Figure 7.1. Multipass welding deposits layers of filler metal that are alternately reheated by the next pass. The result can be complex residual stress distributions created by the partial stress relaxation in the first layer as it is reheated, combined with new tension in the newly deposited layer. Preheating the work before welding is a common means of reducing the thermal strain gradient during weld fusion, and thus the tension created when the weld cools.

Postweld thermal stress relief is commonly used to reduce the tensile stresses created by welding, but complete thermal stress relief can be difficult to achieve. To avoid introducing additional residual stresses from thermal strains, the temperature throughout the component must be uniform during the heating cycle. This is especially important in complex welded assemblies where large thermal stress gradients can develop during heating or cooling. Figure 7.2 shows the residual stress depth profiles for a low carbon steel weld before and after stress relief and shot peening.

Because fatigue and SCC initiate at the surface, the stresses produced by finish machining or grinding can be

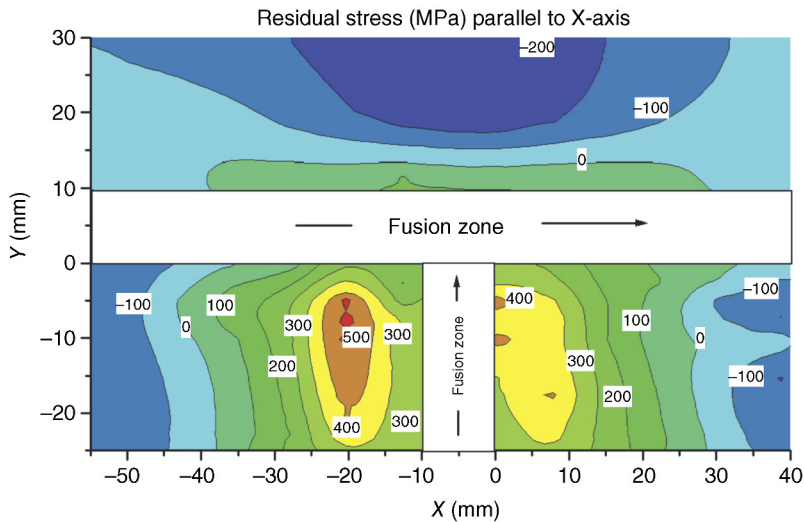


FIGURE 7.1 Contour plot of the surface residual stress distribution in a 304 SS T-Weld.

critically important for subsequent performance. Surface integrity is the discipline dealing with how the condition of the surface, including the residual stress and cold work produced by manufacturing, influences performance in service. Machining and grinding produce residual stress distributions that are shallow, but can be of very high magnitude [5]. The residual stress layer produced is generally less than 0.25 mm deep, but stresses can range from yield strength tension to compression.

Rapid local surface heating is a primary source of highly detrimental residual tension. Machining or grinding practices that quickly heat the surface can produce surface tension and grinder “burn.” The small patch of material at the point of contact with the grinding wheel or cutting tool is quickly heated to incandescence. Local temperatures can be sufficient to cause phase transformations in steels, leaving brittle, cracked, untempered martensite on the surface, a common fatigue initiation mechanism [5]. In any alloy, the locally

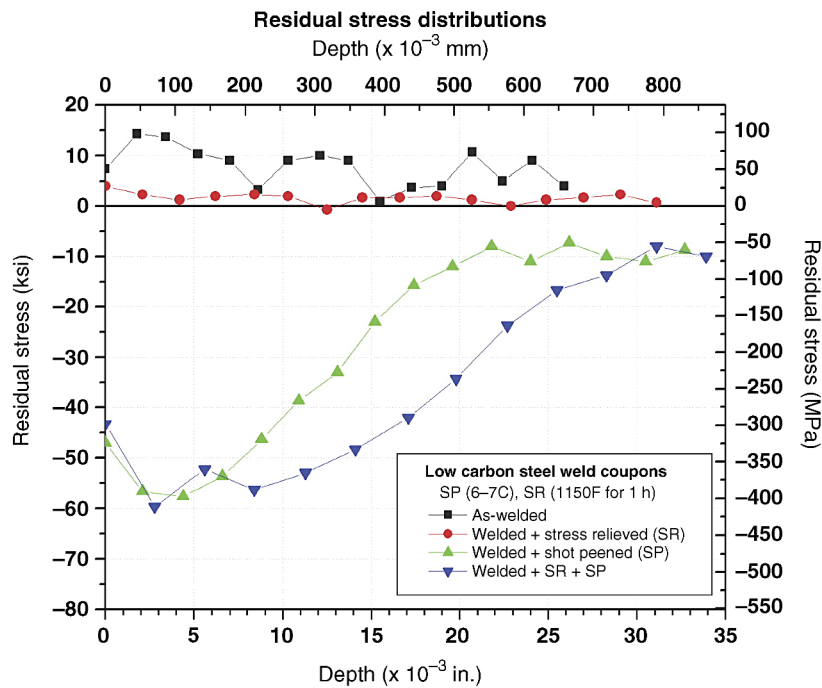


FIGURE 7.2 Residual stress depth distributions for a low carbon steel-butt weld, after thermal stress relief, and shot peening.

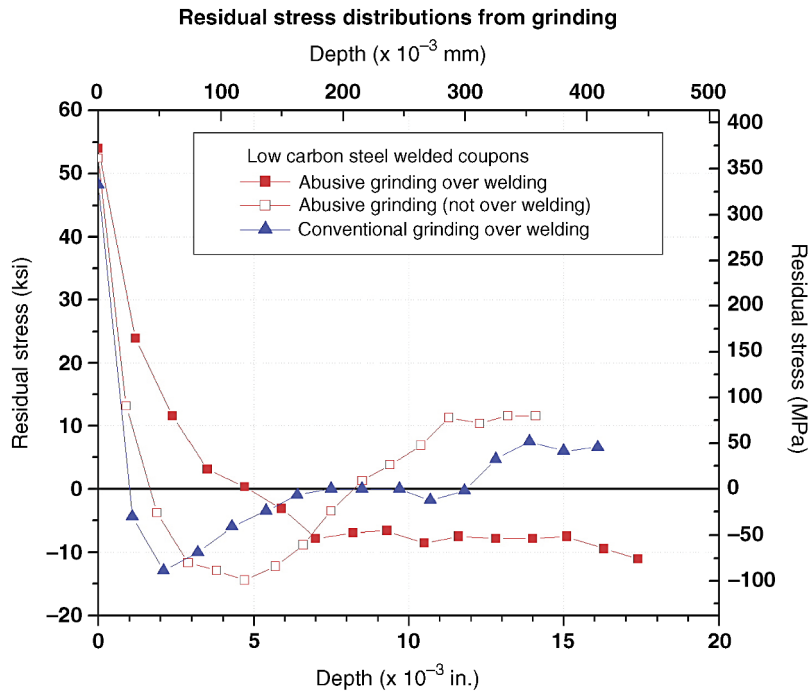


FIGURE 7.3 Subsurface residual stress distributions in ground low carbon steel welds.

heated surface zone expands, but is constrained by the cool material below, briefly creating a compressive thermal stress sufficient to yield the hot zone in compression. When the tool or grinding wheel moves on, the heated zone rapidly cools by self-quenching into the cool substrate material. After yielding in compression when hot, the heated zone is then stretched into tension upon cooling. The residual tension may be so high as to cause surface cracking, forming fatigue and SCC initiation sites.

Cold machining or abrasive operations typically produce shallow, but often high residual compression. Polishing and grinding are chip forming operations on a fine scale that deform the surface in tension, and will produce a shallow layer of surface compression if performed with a liquid coolant so that the surface is not significantly heated. The surface yields in tension as chips are formed, leaving it in residual compression. “Gentle” milling, turning, and similar chip forming operations performed with coolant, sharp tools, shallow depths of cut, and low feeds that minimize heating also leave a compressive surface layer. Wire brushing also produces compression if heat is avoided. Figure 7.3 shows the residual stresses left behind by grinding in low carbon steel weld coupons. Note the high surface tension.

Grinding or machining for weld preparation deserves special mention with regard to pipelines. Weld preparation by hand grinding or machining can highly cold work the surface layer, increasing the yield strength of the material adjacent to the weld. Contraction of the weld upon cooling

then stretches the cold-worked material in the HAZ into high residual tension, leaving the HAZ subject to fatigue or SCC failure in service. This is a primary cause of SCC failures of 304 stainless steel pipe welds made in boiling water nuclear reactor piping.

Installation or “fit-up” stresses are sometimes considered residual stresses in the assembled pipeline or component assembly. Stresses from suspending a pipeline with hangers, loss of support caused by erosion, or flexing of pipe sections in order to make connections before welding or flange joining can be considered to be residual stresses in the completed assembly.

Surface damage in transport, handling, and assembly can produce dents, gouges, cold-worked zones, local areas of high residual stress, and stress concentrations that serve as fatigue and SCC initiation sites [6].

7.2 THE INFLUENCE OF RESIDUAL STRESSES ON PERFORMANCE

The macroscopic residual stresses of concern to engineers are inherently elastic and are additive to applied stresses. Residual stresses remain in equilibrium in the body indefinitely after creation by thermal-mechanical processes that cause nonuniform plastic deformation. In the case of pipelines, stresses from pressurization, suspended loads, vibration during operation from pumping cycles, earthquakes, soil settling, and so on would be directly summed with existing

residual stresses in the pipe. Pipelines are subject to failure in service primarily by fatigue, SCC, or corrosion fatigue (CF), all of which require a net tensile stress at the surface for initiation. Tensile residual stresses from any origin render the pipeline more likely to fail, whereas compressive stresses are generally beneficial. It is useful to consider how residual stresses influence each of these failure mechanisms separately.

7.2.1 Fatigue

Fatigue failure is caused by cyclic loading to stress levels above the endurance limit of the material. Cracks initiate at the surface or from some internal flaw, such as an inclusion in the metal. Stress concentrations such as corrosion pits or scratches due to handling are common initiation sites. Fatigue is classified as low cycle fatigue (LCF) or high cycle fatigue (HCF), depending upon the stress level and number of cycles to failure. In LCF, the maximum alternating stress exceeds the proportional limit causing plastic deformation. Cracks initiate immediately, and life is determined by crack propagation, usually in tens of thousands of cycles or less. Cyclic plastic deformation in LCF reduces the effect of any residual stresses, and even applied mean stresses. HCF occurs more commonly in pipelines, under essentially elastic cyclic loading, and failures occur only after 10^5 or more cycles. Residual stresses add to the mean applied stress during fatigue, and can strongly influence HCF performance. Welding residual stresses have a dominant influence on the mean stress and fatigue performance in pipelines [7]. Once a pipeline is assembled and in operation, the vibratory stresses contributing to fatigue are generally so small that only HCF needs to be considered.

All fatigue failures initiate in shear, and will invariably initiate at the surface of a body under cyclic load because the shear stresses are maximum at the free surface. When the maximum stress is raised to the fatigue endurance limit, those few crystals on the surface of a pipeline that happen to be favorably oriented to exceed the critically resolved shear stress (i.e., having slip planes tipped 45° into the direction of loading) will begin to ratchet on slip planes with each loading cycle. Dislocations are pumped along the slip planes, alternately forming notches and extruding metal slightly from the surface. After the majority of the fatigue life in HCF, the ratcheting process eventually creates a notch on the order of a full crystalline grain. Fatigue cracks then grow from the notch, and propagate by the rules of fracture mechanics to failure in the final stages of the fatigue process.

The contribution of mean stresses and residual stresses to fatigue performance can be understood in terms of the Haigh diagram. The alternating stress allowed for a given fatigue life is plotted on the vertical axis as a function of the mean stress, plotted on the horizontal axis, which ranges from tension to compression. The sum of the alternating and mean

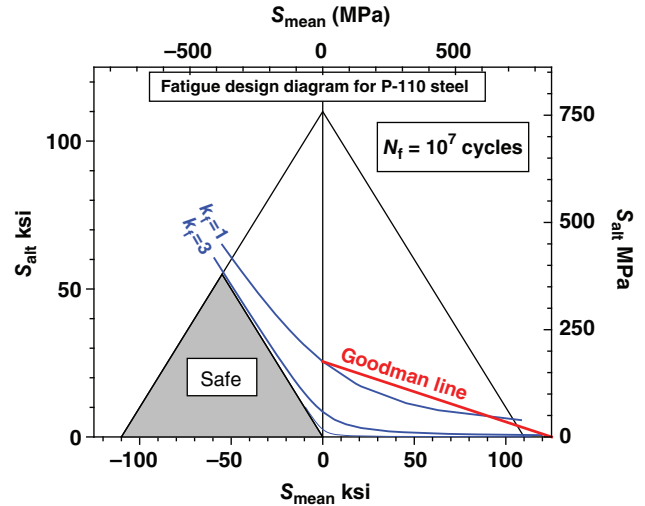


FIGURE 7.4 Fatigue design diagram for P110 steel.

stress is limited to the material yield strength at the triangular boundary. The Goodman line, an estimate for only tensile mean stresses, is plotted from the fully reversed (zero mean stress) fatigue strength to the ultimate strength. An example for P110 steel oil field tubulars for a fatigue life of 10^7 cycles is shown in Figure 7.4. The Smith–Watson–Topper curve plotted for no damage, $k_f = 1$, gives the upper bound for the allowed alternating stress with mean stresses extended into compression. Adding Neuber’s rule to account for damage provides a fatigue design diagram (FDD) useful for determining the amount of compression needed to mitigate damage [8]. The mean stress is the sum of the applied mean stress and the residual stresses at the surface of the pipe. In pipeline applications, the alternating stress could be the magnitude of the transient stress from vibrations or pressure pulsations from a pumping station.

The FDD shows that under applied mean or residual compression, the allowed alternating stress increases significantly, a great benefit in fatigue. Damage increases k_f , reducing the allowed alternating stress with positive mean stress. The allowed alternating stress must be less than the $k_f = 3$ curve for a 10^7 cycle life when damage reduces the fatigue strength to one-third of the original. Even with severe damage, such as an existing fatigue crack, if the sum of residual and applied mean stresses moves the operating condition into the gray triangle labeled “SAFE,” the material is always in compression, and fatigue cracks cannot grow. Any surface, even with fatigue-initiating damage, operating within this safe triangle cannot fail in fatigue. This is the basis for introducing beneficial residual compression using surface enhancement treatments. The maximum possible alternating stress is achieved at the center of the “SAFE” triangle with the net mean stress, residual plus applied, equal to half of the yield strength.

7.2.2 Stress Corrosion Cracking

Stress corrosion cracking (SCC) refers to the propagation of cracks under a static tensile load in the presence of a chemically active environment to which the material is susceptible. SCC is also termed “environmentally assisted” cracking. Ferritic pipeline steels can be subject to hydrogen sulfide (H₂S) SCC or “sulfide stress cracking” (SSC) in sour well environments [9,10]. Carbonate (CO₃) cracking is also possible and chloride SCC is common to many alloys, notably stainless steels, and is exacerbated by tensile residual stresses [11]. Pipelines transporting ethanol, even as a minor fraction mixed with petroleum products, are subject to internal SCC due to the affinity of ethanol for water and the ability of ethanol to support corrosion [12]. The combination of chemical and mechanical elements makes SCC more complex, and less well understood, than fatigue. The mechanisms and occurrence of SCC in various alloys and environments are discussed in detail elsewhere in this volume.

SCC can only occur if three conditions are met, as shown schematically in the Venn diagram in Figure 7.5. First, the material must be susceptible to cracking in the service environment. Second, the material must be exposed to the chemically active environment with the ions present that will cause cracking to occur. And third, there must be a tensile stress, residual plus applied, present at the surface of the material that exceeds some threshold level.

A possible, but often prohibitively expensive, way to mitigate SCC is to replace the alloy with one that is not susceptible in the environment. In the case of ferritic steels, the use of lower strength grades with higher fracture toughness can reduce the propensity to fracture, but with the performance limitations of the lower strength. A protective

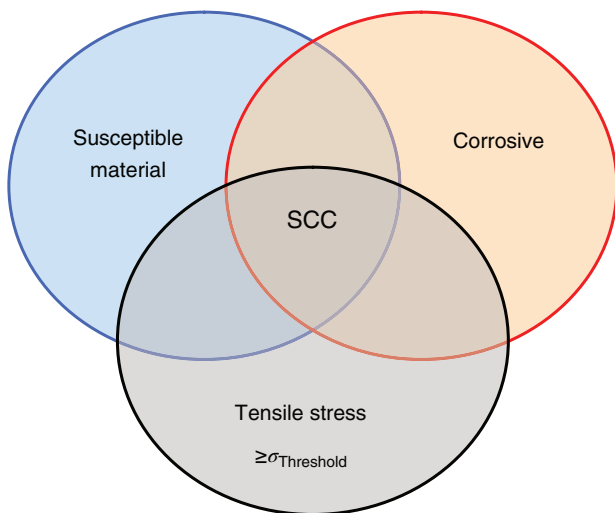


FIGURE 7.5 Venn diagram of SCC contributors: material, environment, and tension.

coating can be used to isolate the surface from the chemical environment, but the coating may be breached, allowing failure.

As in the case of fatigue, residual stresses influence SCC by being additive to the mean stresses applied to the pipeline. If a tensile residual stress, for example, from welding, added to the applied stress exceeds the threshold for SCC for that material and exposure, cracking can be expected to occur. Welding procedures and parameters can be modified to control the magnitude and distribution of residual stresses developed by pipeline welding [13]. If the surface that is in contact with the environment is kept in compression by a layer of residual stress, SCC can be eliminated. It may be possible to control welding methods to produce compressive residual stresses in the pipe [14]. In addition to inter- and transgranular SCC cracking, corrosion pitting has been reported to occur preferentially in areas with the highest tensile residual stress [15].

7.2.3 Corrosion Fatigue

Corrosion fatigue is the combination of mechanical fatigue-generated cracks that are further propagated in a chemically aggressive environment by SCC. The fatigue strength of many alloys is reduced by exposure to chloride solutions, generally salt water. In fatigue with the absence of corrosion, many alloys, including pipeline steels, will exhibit an endurance limit. Below this cyclic stress level, fatigue cracks will not initiate, and the fatigue life is essentially infinite. A prominent effect of corrosion fatigue, illustrated in the case studies section, is the elimination of any endurance limit, so that fatigue cracks propagate even at very low alternating stress levels. In high-strength steels, the loss of fatigue strength in the presence of a corrosive environment can be spectacular. High-strength 300M steel exposed to 3.5% NaCl solution has only 20% of the fatigue strength of baseline material at 10^7 cycles, with no evident endurance limit. As in simple fatigue or static SCC, the presence of residual stresses adds to the mean stress, and can either exacerbate or mitigate SCC. The corrosion debit during fatigue in pipeline steels requires tension exceeding a threshold level, and is mitigated by reducing tensile or introducing compressive residual stress [15].

7.2.4 Effects of Cold Working and Microscopic Residual Stresses

Any polycrystalline metal, such as pipeline steel, when mechanically processed by grinding, machining, bending, flaring, weld shrinkage, or other mechanical means will necessarily be plastically deformed to some degree. Even a delicate metallographic polishing process is a chip forming grinding operation on a microscopic scale, plastically deforming the surface to a shallow depth. Plastic deformation

of metals forms vast numbers of dislocations along slip planes in the individual grains or crystals of the metal. The increase in dislocation density changes the properties of the metal in ways that can be as important as the macroscopic residual stresses. The degree of plastic deformation can be quantified during X-ray diffraction (XRD) residual stress measurement as an increase in X-ray peak broadening, while the macroscopic residual stress causes a shift in the peak position.

Cold working influences the corrosion behavior of many metals, leaving the deformed surface more chemically active. For example, cold working of P110 steel casing reduces the open-circuit potential (OCP) in salt water, effectively making the metal less noble than chemically identical P110 material that is not so severely cold worked. The cold-worked areas corrode preferentially and faster than the undisturbed material. The corrosion rates of pipeline steels have been shown to increase with cold working in sour gas (H_2S) environments [16,17].

Cold working influences the stability of residual stresses at elevated temperatures. Once the dislocation density of the material becomes high enough, residual stresses can relax extremely rapidly by dislocation annihilation. This effect can result in the loss of beneficial compression introduced by shot peening or other mechanical working processes that introduce high levels of cold work [18].

Cold working and the resulting dislocation density produce an increase in the yield strength of many materials. A surface cold worked by shot peening or other means will have a variation in yield strength with depth through the deformed layers, from the highly cold-worked surface to the unworked interior. Austenitic alloys, like stainless steels, can have a 400% increase in yield strength from surface work hardening. If a surface layer of cold-worked metal is then deformed, as may occur in the weld HAZ during cooling and contraction, the metal will yield different amounts at each depth, depending upon the state of residual stress and the yield strength in each layer. A compressive surface layer produced by shot peening or low stress grinding can be left in residual tension after subsequent deformation.

Because cold working can alter mechanical behavior, unnecessary cold working should be avoided. Austenitic alloys with face-centered cubic structures are particularly susceptible to work hardening. Minimizing cold work ensures that the finished pipeline or component will behave in a manner to be expected for the base material properties.

7.3 RESIDUAL STRESS MEASUREMENT

This section is intended to introduce the pipeline engineer to the practical methods of residual stress determination that should be considered in the event that measurement is necessary, and to support understanding of residual stress

studies presented in the literature. The advantages, disadvantages, and limitations of the established methods are described. Methods that have been investigated but remain largely in the laboratory and are of limited use to a pipeline engineer are not included. The reader is referred to handbooks with comprehensive chapters covering the various methods for detailed discussion of the practical techniques and experimental methods [19,20].

Although commonly used, the phrase “residual stress measurement” is actually a misnomer. Stress, like density, is an extrinsic property that cannot be directly measured, but can only be calculated from measurable properties. Residual stress measurement or determination methods can be considered to be in two categories: those that measure strain and calculate the stress by linear elasticity theory, and those that utilize some other property influenced by residual stress, such as magnetic or acoustical behavior.

The linear elastic methods that measure strain, or changes in strain, and calculate the stress using elasticity theory include the mechanical and diffraction methods. Residual stresses are necessarily entirely elastic once the body is in equilibrium, so the residual strain is proportional to the residual stress.

The first group of linear elastic mechanical methods includes all of the dissection methods of slitting, sectioning, center hole drilling, and ring core or trepanning that use electrical resistance or mechanical strain gauges to measure the change in strain as residual stresses are relaxed. The residual stresses present before sectioning are calculated from these strain measurements. Most of the layer removal and slitting methods rely upon simplifying assumptions of component geometry and stress field to facilitate solution. Only the portion of the residual stress that is relaxed can be calculated, and care must be taken not to introduce residual stresses during sectioning.

The second group of linear elastic methods includes the X-ray diffraction (including synchrotron) and neutron diffraction techniques. In the diffraction methods, the strain is measured between planes of atoms in the crystals of the metal, in this case the pipeline steel. Tension will increase and compression will decrease the lattice spacing in the direction of the stress. The residual stress is calculated from the strain measured in the crystal lattice. The diffraction techniques are nondestructive, but require sampling of a large number of small crystals to provide an accurate statistical average of the macroscopic residual stress. Measurement in coarse-grained material, such as castings and weld fusion zones, can be difficult. Conventional X-ray diffraction penetration is very shallow, providing only surface values without removing material. Neutron and synchrotron penetration can be up to centimeter and millimeter, respectively, but require highly specialized facilities and independent knowledge of the unstressed lattice spacing to calculate the stress present.

Residual stress measurement by mechanical methods involves removing or sectioning material to relieve a portion of the residual stress, and measuring the resulting change in strain or material displacement, from which the stress is calculated. These methods can be categorized as destructive or semidestructive depending upon the relative amount of material removed. Displacements are typically measured with electrical resistance strain gauges. Air gauge and optical systems can also be used to measure material displacements. The residual stress that was relaxed by sectioning is then calculated using equations developed usually assuming some symmetry to the residual stress field to allow algebraic solution. Both sectioning and hole drilling methods are commonly applied to welded pipelines [21]. For the general application, semidestructive mechanical measurement methods such as center hole drilling and ring core are preferred because symmetry of the residual stress field is not required.

The nonlinear elastic techniques form the other major class of residual stress determination methods. These include magnetic and ultrasonic techniques, where pressure- or stress-sensitive changes in properties other than strain are measured. All of these require measurement of some nonlinear, often high-order effect with high accuracy. All are strongly influenced by other material properties, such as hardness, dislocation density, and crystal orientation, and interpretation of the residual stress contribution is very difficult in practice. The Barkhausen noise magnetic method is the only nonlinear elastic method that will be further considered here [22].

7.3.1 Center Hole Drilling Method

The center hole drilling method [20,23,24] is a mechanical technique that allows the determination of bulk or incremental residual stress versus depth. Hole drilling involves introducing a small hole at the center of a specially designed three- or six-element strain gauge and measuring the resulting strain relaxation, as shown schematically in Figure 7.6. Depths of

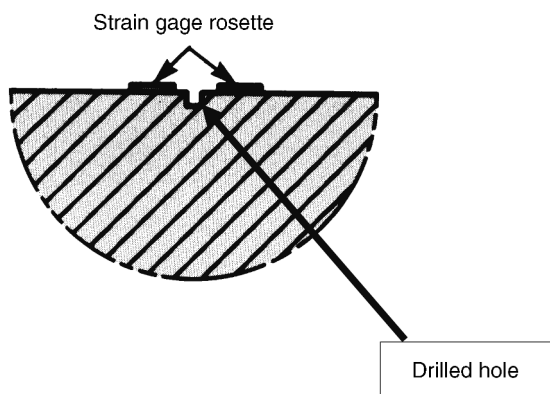


FIGURE 7.6 Schematic of center hole drilling test.

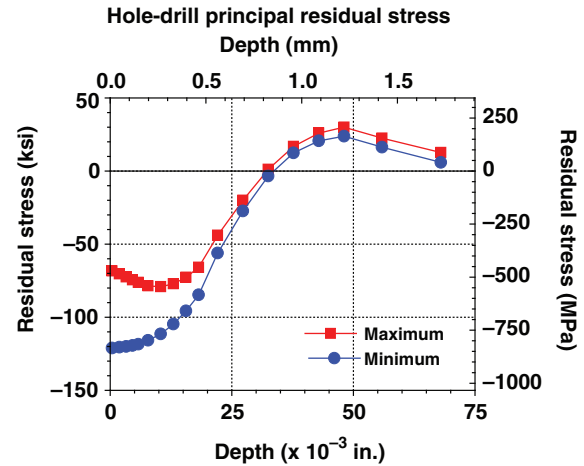


FIGURE 7.7 Example of hole drilling data set.

up to 2 mm (0.08 in.) can typically be measured with this method. The hole drilling method is often referred to as semidestructive because the hole that is introduced does not significantly affect the usefulness of the work piece for some applications, or may be repaired after measurement. It has been used extensively for both laboratory and field studies of residual stresses, including welding stresses in pipe [21].

Principal residual stresses and their angular orientation are determined from the relaxed strain and calibration coefficients for each specific strain gauge geometry and hole size. An example of the subsurface principal residual stress distributions produced by low plasticity burnishing[®] (LPB) on a test coupon and measured by the incremental center hole drilling method is shown in Figure 7.7.

The hole drilling procedure has been standardized in ASTM Standard Test Method E837 under the auspices of Subcommittee E28.13 on residual stress measurement [23]. This method applies in cases where material behavior is linear elastic. In theory, it is possible for local yielding to occur due to the stress concentration around the drilled hole when the residual stress exceeds nominally half of the yield strength, and stresses calculated to be significantly higher may be subject to higher experimental error. The theoretical basis, underlying assumptions and limitations, are most thoroughly developed in Micro-Measurements Tech Note TN-503, which is strongly recommended as a training guide [24].

Hole-drilling equipment and supplies are commercially available and a qualified stress technician can successfully perform the test by adhering to the ASTM standard. Tests can be performed either in a laboratory or in the field on components with a variety of sizes and shapes.

7.3.2 Ring Core Method

The ring core or trepanning [25–27] is another mechanical residual stress measurement method that allows for deeper

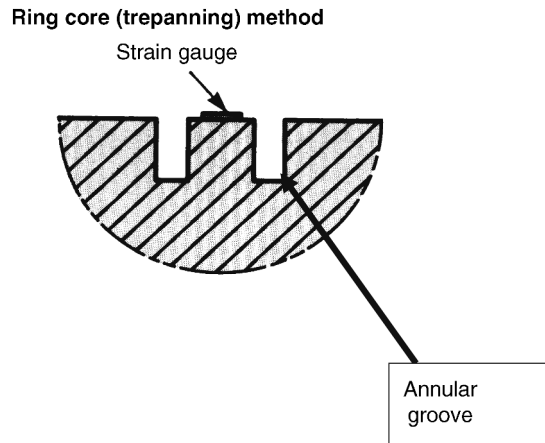


FIGURE 7.8 Schematic of ring core test.

residual stress measurements to be made compared with the hole drilling method. The ring core method involves introducing an annular groove around a three-element strain gauge. Because the cylindrical core is completely separated from the rest of the component, more of the residual strain is relaxed, and the ring core technique can provide nominally an order of magnitude greater measurement sensitivity than hole drilling. The cylindrical core containing the strain gauge is relaxed and the resulting strain relaxations are measured. Because there is no stress concentration at the gauge, residual stresses up to the yield strength can be measured accurately. Principal residual stresses and their angular orientation at each depth are determined from the relaxed strain using relaxation coefficients determined by calibration or finite element calculation. Figure 7.8 is a schematic of the basic ring core setup.

Depths of up to 5 mm (~0.2 in.) can typically be measured in a single ring core. Measurement depth can be increased through the use of larger diameter coring tools; however, resolution is reduced as a trade-off. Although the strain response attenuates with greater depths, there is a limit to which residual stresses can be measured. In order to collect deeper residual stresses, the cylindrical post can be removed and a new strain gauge applied to continue further in depth. An example of the principal residual stress distributions measured by the incremental ring core method in a welded 304 SS sample is shown in Figure 7.9.

7.3.3 Diffraction Methods

In X-ray diffraction residual stress measurement, the strain in the crystal lattice is measured directly and the residual stress producing the strain is calculated, assuming a linear elastic distortion of the crystal lattice. The basic “sine-squared psi” method was well developed by the SAE Fatigue Design and Evaluation Committee in the 1960s, and the reader is referred to SAE HS784 for details of the theoretical basis and

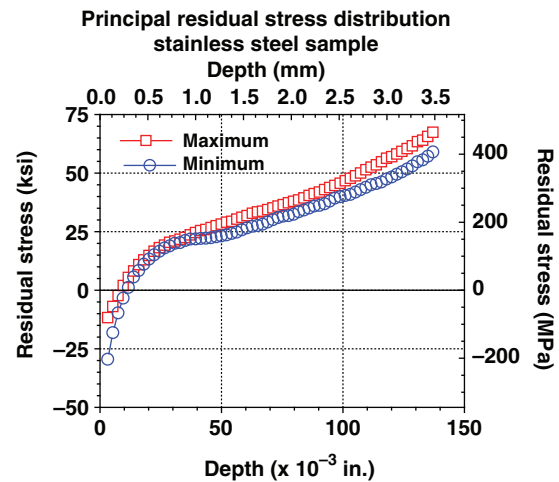


FIGURE 7.9 Example of ring core data set.

practical experimental techniques [28]. XRD is the only nondestructive method that determines residual stress directly from measured strain that can be used in the field or laboratory with commercially available apparatus. The pipeline engineer interested in determining residual stress will benefit by understanding the similarity of XRD to mechanical elasticity-based methods. Therefore, a brief overview with derivation from linear elasticity theory is presented.

X-ray diffraction residual stress measurement is applicable to materials that are crystalline and relatively fine grained and that produce diffraction for any orientation of the sample surface. To determine the stress, the strain in the crystal lattice must be measured for at least two orientations relative to the sample surface. Samples may be metallic or ceramic, provided a diffraction peak of suitable intensity and free of interference from neighboring peaks can be produced in the high back-reflection region with the radiations available. X-ray diffraction residual stress measurement is unique in that macroscopic and microscopic residual stresses can be determined nondestructively and separately from the diffraction peak position and breadth, respectively.

7.3.3.1 Principles of X-Ray Diffraction Stress Measurement Figure 7.10 shows the diffraction of a monochromatic beam of X-rays at a high diffraction angle (2θ) from the surface of a stressed sample for two orientations of the sample relative to the X-ray beam. The angle ψ , defining the orientation of the sample surface, is the angle between the normal of the surface and the incident and diffracted beam bisector, which is also the angle between the normal to the diffracting lattice planes and the sample surface.

Diffraction occurs at an angle 2θ , defined by Bragg's law: $n\lambda = 2d \sin \theta$, where n is an integer denoting the order of diffraction, λ is the X-ray wavelength, d is the lattice spacing of crystal planes, and θ is the diffraction angle. For the

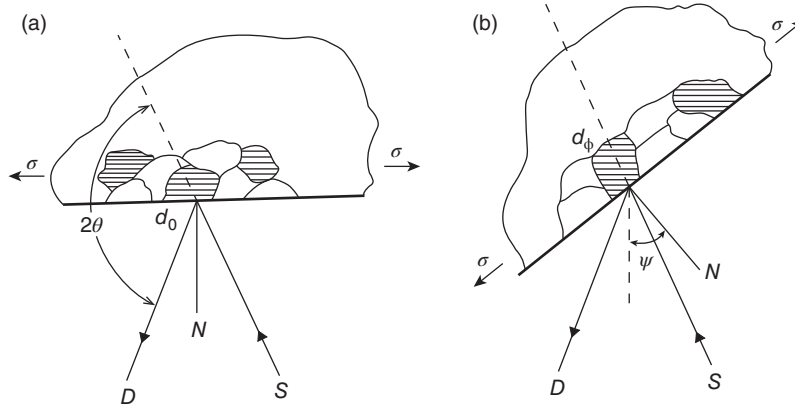


FIGURE 7.10 Principles of X-ray diffraction stress measurement. (a) $\psi = 0$. (b) $\psi = \psi$ (sample rotated through some known angle ψ). D: X-ray detector; S: X-ray source; N: normal to the surface.

monochromatic X-rays produced by the metallic target of an X-ray tube, the wavelength is known to be 1 part in 10^5 . Any change in the lattice spacing d results in a corresponding shift in the diffraction angle 2θ .

Figure 7.10a shows the sample in the $\psi = 0$ orientation. The presence of a tensile stress in the sample results in a Poisson's ratio contraction, reducing the lattice spacing and slightly increasing the diffraction angle 2θ . If the sample, or apparatus, is then rotated through some known angle ψ (Figure 7.10b), the tensile stress present in the surface increases the lattice spacing over the stress-free state and decreases 2θ . Measuring the change in the angular position of the diffraction peak for at least two orientations of the sample defined by the angle ψ enables calculation of the stress present in the sample surface lying in the plane of diffraction, which contains the incident and diffracted X-ray beams. To measure the stress in different directions at the same point, the sample is rotated about its surface normal to coincide the direction of interest with the diffraction plane.

The residual stress determined using X-ray diffraction is the arithmetic average stress in a volume of material defined by the irradiated area, which may vary from square centimeters to square millimeters, and the depth of penetration of the X-ray beam. The linear absorption coefficient of the material for the radiation used governs the depth of penetration, which can vary considerably. In steels, 50% of the radiation is diffracted from a layer approximately 0.005 mm (0.0002 in.) deep for the Cr K_α radiation generally used for stress measurement. Electropolishing is used to remove thin layers to expose new surfaces for subsurface measurement.

7.3.3.2 Plane Stress Elastic Model X-ray diffraction stress measurement is confined to the surface of the sample in a layer so thin that a condition of plane stress is assumed to exist. That is, a stress distribution described by principal stresses σ_1 and σ_2 exists in the plane of the surface, and no stress is assumed perpendicular to the surface, $\sigma_3 = 0$.

However, a strain component perpendicular to the surface, ϵ_3 , exists as a result of the Poisson's ratio contractions caused by the two principal stresses, shown in a three-dimensional view in Figure 7.11.

The strain, $\epsilon_{\phi\psi}$ in the direction defined by the angles ϕ and ψ is

$$\epsilon_{\phi\psi} = \left[\frac{1 + \nu}{E} \sigma_\phi \sin^2 \psi \right] - \left[\left(\frac{\nu}{E} \right) (\sigma_1 + \sigma_2) \right] \quad (7.1)$$

where E is the modulus of elasticity, ν is the Poisson's ratio, and σ_ϕ is the stress of interest in the surface.

If $d_{\phi\psi}$ is the spacing between the lattice planes measured in the direction defined by ϕ and ψ , the strain can be expressed in terms of changes in the linear dimensions of the crystal lattice:

$$\epsilon_{\phi\psi} = \frac{\Delta d}{d_0} = \frac{d_{\phi\psi} - d_0}{d_0} \quad (7.2)$$

where d_0 is the stress-free lattice spacing.

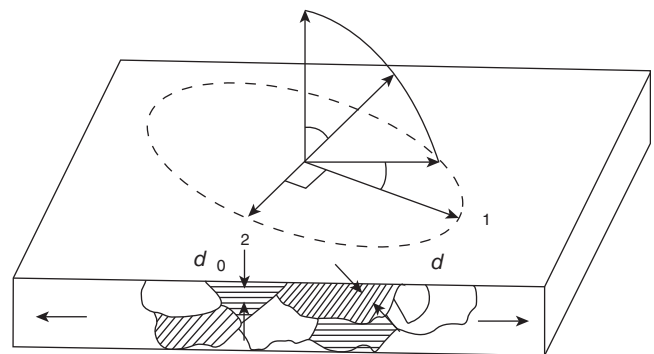


FIGURE 7.11 Plane stress elastic model.

Substituting for strain in the crystal lattice, the lattice spacing for any orientation, then, is

$$d_{\phi\psi} = \left[\left(\frac{1+\nu}{E} \right)_{(hkl)} \sigma_{\phi} d_0 \sin^2 \psi \right] - \left[\left(\frac{\nu}{E} \right)_{(hkl)} d_0 (\sigma_1 + \sigma_2) + d_0 \right] \quad (7.3)$$

This is the fundamental relationship between lattice spacing and the biaxial stresses in the surface of the sample. The elastic constants $(1 + \nu/E)_{(hkl)}$ and $(\nu/E)_{(hkl)}$ are not the bulk values, but the values for the crystallographic direction normal to the lattice planes in which the strain is measured, as specified by the Miller indices (hkl) . Because of elastic anisotropy, the elastic constants in the (hkl) direction commonly vary significantly from the bulk mechanical values.

The lattice spacing $d_{\phi\psi}$ is then a linear function of $\sin^2 \psi$. If the lattice spacing is measured at two or more angles ψ (two-angle or sine-squared psi methods), then the slope of the plot is

$$\frac{\partial d_{\phi\psi}}{\partial \sin^2 \psi} = \left(\frac{1+\nu}{E} \right)_{(hkl)} \sigma_{\phi} d_0 \quad (7.4)$$

Solving for the stress of interest, σ_{ϕ} is

$$\sigma_{\phi} = \left(\frac{E}{1+\nu} \right)_{(hkl)} \frac{1}{d_0} \left(\frac{\partial d_{\phi\psi}}{\partial \sin^2 \psi} \right) \quad (7.5)$$

The X-ray elastic constants can be determined empirically, but the unstressed lattice spacing d_0 varies with alloy composition and cold working, and is generally unknown. However, because for metals, $E \gg (\sigma_1 + \sigma_2)$, the value of $d_{\phi=0}$ differs from d_0 by not more than $\pm 1\%$ and σ_{ϕ} may be approximated to that accuracy using

$$\sigma_{\phi} = \left(\frac{E}{1+\nu} \right)_{(hkl)} \frac{1}{d_{\phi 0}} \left(\frac{\partial d_{\phi\psi}}{\partial \sin^2 \psi} \right) \quad (7.6)$$

The method then becomes a differential technique and no stress-free reference standards are required to determine d_0 for the biaxial stress case. This is a significant advantage over synchrotron and neutron diffraction methods that must assume a three-dimensional stress state, and therefore require independent knowledge of the unstressed crystal lattice spacing in order to calculate the stress tensor from the measured strains.

Because the depth of material sampled is very shallow, any secondary abrasive treatment, such as wire brushing or sand blasting, radically alters the surface residual stresses, generally producing a shallow, highly compressive layer completely altering the original residual stress distribution.

To measure inaccessible locations, such as the inside surface of pipes and tubing, the sample must be sectioned to provide clearance for the diffraction apparatus and the incident and diffracted X-ray beams. Unless prior experience with the sample under investigation indicates that no significant stress relaxation occurs upon sectioning, electrical resistance strain gauge rosettes should be applied to the measurement area to record the strain relaxation that occurs during sectioning. Following X-ray diffraction residual stress measurements, the total stress before sectioning can be calculated by subtracting the sectioning stress relaxation from the X-ray diffraction results.

7.3.3.3 Sources of Error Geometric precision is required for diffraction techniques. Because the diffraction angles must be determined to accuracies of nominally $\pm 0.01^\circ$, the sample must be positioned in the X-ray beam at the true center of rotation of the ψ and 2θ axes and the angle ψ must be known and constant throughout the irradiated area. Precise positioning of the sample to accuracies of approximately 0.025 mm (0.001 in.) is critical. The size of the irradiated area must be limited to an essentially flat region on the sample surface.

Instrument alignment requires coincidence of the θ and ψ axes of rotation and positioning of the sample such that the diffracting volume is centered on these coinciding axes. Instrument alignment can be checked readily using a stress-free powder sample [29]. If the diffraction apparatus is properly aligned, a loosely compacted stress-free powder sample should indicate not more than ± 14 MPa (± 2 ksi) apparent stress.

Excessive sample surface roughness or pitting, curvature of the surface within the irradiated area, or interference of the sample geometry with the diffracted X-ray beam can result in systematic error. Residual stress generally cannot be measured reliably using X-ray diffraction in samples with coarser-grain sizes, common in castings and weld beads.

A major source of potential systematic proportional error arises in determination of the X-ray elastic constants $(E/(1 + \nu))_{(hkl)}$. The residual stress calculated is proportional to the value of the X-ray elastic constants, which may differ by as much as 40% from the bulk value due to elastic anisotropy. The X-ray elastic constant can be determined empirically by loading a sample of the material to known stress levels and measuring the change in the lattice spacing as a function of applied stress and ψ tilt [30,31]. The X-ray elastic constant can then be calculated from the slope of a line fitted by least-squares regression through the plot of the change in lattice spacing for the ψ tilt used function of applied stress. X-ray elastic constants for many steels have been published.

X-ray diffraction measures the entire strain present before any sectioning or removal of material, but the shallow penetration requires removal of layers to expose the sub-surface material for strain measurement. There are two

important corrections that must be applied to subsurface measurements. First, in the presence of a steep stress gradient, as is common on machined or ground surfaces, the exponential attenuation of X-rays penetrating the layers of varying stress gives a weighted average stress that can be unfolded if measurements are made in sufficiently fine layers. Second, the removal of stressed material alters the residual stress in the exposed layers, causing an error that accumulates with depth, but can be corrected with an integral solution analogous to the layer removal mechanical residual stress measurement methods. Appropriate corrections for both sources of error in subsurface measurement are well established and described in SAE HS784 [28].

7.3.4 Synchrotron X-Ray and Neutron Diffraction: Full Stress Tensor Determination

Conventional X-ray diffraction stress determination uses low-energy, shallow-penetrating radiation allowing stress determination in the biaxial case, eliminating the need for a stress-free reference sample to calculate the residual stress. This is a major advantage, allowing reliable measurement in materials, such as welds, with local variation in composition. In principle, the full tensor can be determined non-destructively using either high-energy synchrotron X-radiation or thermal neutrons from a suitable reactor source. Both synchrotron X-ray and neutron diffraction methods have been developed for determining the full triaxial stress tensor [20]. Penetration depths can range from millimeter for synchrotron X-rays to centimeter for thermal neutrons. Both require expensive stationary facilities generally available only at major government laboratories. In all other respects, both are diffraction techniques measuring lattice strain, and are subject to the same limitations and error sources as the conventional, portable, plain stress biaxial X-ray method.

Unlike the plane stress X-ray method, determination of the triaxial stress tensor requires independent knowledge of the unstressed lattice spacing d_0 at the accuracy required for strain measurement (1 part in 10^5) to calculate the residual stress from the measured strains. It is not possible to solve for three-dimensional stresses from the measured strains without separate knowledge of the unstressed lattice spacing as a zero-stress reference. Unfortunately, the unstressed lattice spacing varies with cold working (due to dislocation density) and local variation in chemical composition. In many cases, including surfaces plastically deformed by machining, weld fusion and heat-affected zones, or in case-hardened carburized steels, the lattice spacing varies as a result of deformation, composition, or heat treating, precluding independent determination of the unstressed lattice spacing with sufficient precision to make reliable stress tensor calculations.

The equipment requirements, lack of portability, extensive data collection required, and dependence on absolute knowledge of d_0 limit the full tensor method primarily to

research applications. Mechanical methods, primarily center hole drilling and ring core, or conventional plane stress biaxial X-ray diffraction methods, are recommended for general use for determining the residual stress distributions in pipelines.

7.3.5 Magnetic Barkhausen Noise Method

The Barkhausen Noise method [20,32] is a nondestructive, high-speed technique applicable to ferritic materials and, therefore, well suited for steel pipe inspections [33]. The Barkhausen technique relies upon analyzing the “noise” observed on the magnetic hysteresis loops when an alternating current is used to alternately magnetize the metal in North–South and South–North orientations. A pickup coil then detects the resultant magnetic field. The individual magnetic domains within the crystalline grains that make up the material are typically oriented in alternating N–S and S–N orientations. Under stress, the domains can flip their orientation, resulting in changes in the magnitude of the noise imposed upon the magnetic hysteresis loop, shown schematically in Figure 7.12. This noise must be analyzed by electronically separating and filtering a certain frequency range that is sensitive to stress. As noted below, the noise level is affected by a variety of other metallurgical properties, such as hardness, grain size, and texture (preferred orientation), the effects of which must be separated from that of residual stress.

The Barkhausen noise level is expressed as a “magnetoelastic parameter” (MP), defined as the root mean square (RMS) level of the Barkhausen noise after amplification and filtering, relative to the unstressed state of the material. The depth of the material sampled is attenuated exponentially with depth, and diminishes with increasing frequency. The depth of penetration is governed by the “skin” effect.

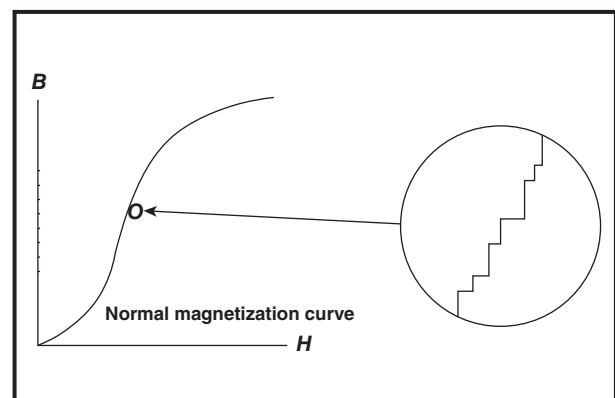


FIGURE 7.12 Barkhausen noise caused by magnetic domain reversals on the magnetization hysteresis curve for steel [19]. (Reproduced with kind permission from Society for Experimental Mechanics, Inc.)

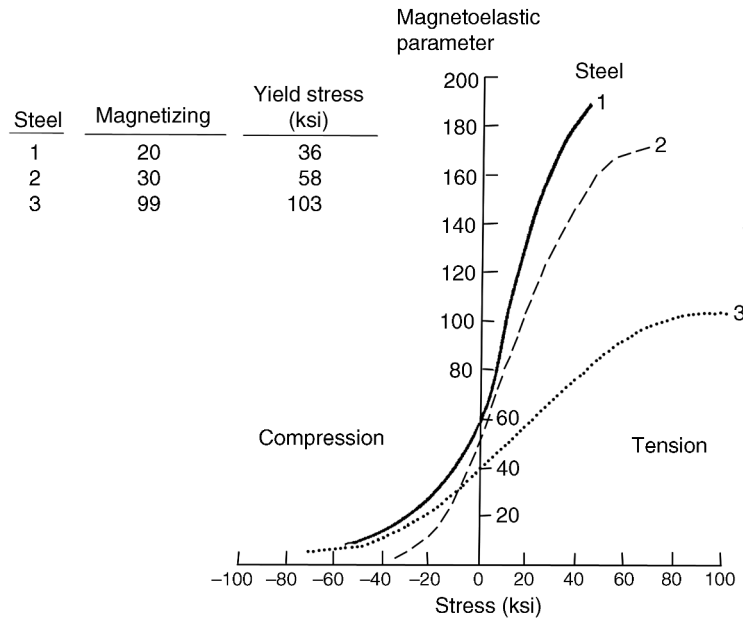


FIGURE 7.13 Barkhausen MP calibration curves for steels of different hardness and yield strength showing nonlinearity, higher sensitivity to tensile stress, and reduced sensitivity at higher strengths.

Excitation frequencies from 3 to 15 kHz provide a depth of penetration of nominally 0.20 mm. Higher frequencies of 70–200 kHz sample shallower depths on the order of 0.02 mm. Barkhausen provides a sampling depth between that of the shallower X-ray diffraction and the deeper hole drilling or ring core mechanical techniques. The maximum range of penetration reportedly ranges from 0.10 to 3.0 mm for the practical frequencies and instrumentation.

The Barkhausen noise response to stress is asymmetric, being larger for tensile stresses and less sensitive to compression. The response curve is a general sigmoid “S” shape, shown in Figure 7.13. The magnetoelastic parameter (MP) is higher for softer, more easily magnetized low-strength steels, and lower for harder, higher strength steels. Calibration is required for the material, frequency, noise analysis (filtration) method, and instrumentation used. Individual transducers may not be interchangeable, so calibration using strain gauge beams or pipe sections loaded to known stress levels is recommended for each instrument and application.

The Barkhausen technique is sensitive to a range of material properties other than strain, as is true of virtually all of the nonlinear-elastic measurement methods. Barkhausen is sensitive to the grain size of the material. For fine-grained material, the MP initially increases rapidly with grain size, and then less rapidly for larger grains. Texture, or the crystallographic orientation, strongly influences the Barkhausen technique, which samples the switching of the direction of magnetization of magnetic domains along the specific crystallographic directions. Hardness and yield strength of the material have a strong influence, as seen in

Figure 7.13. The hardness dependence is so pronounced that the same Barkhausen technology used for stress measurement is used to distinguish hardness and detect grinder burn in steels. The MP level for a given tensile stress can range from nearly a factor of 4, from a high output of 200 for soft 35 HRC steel, to as low as 50 for fully hardened 60 HRC material. The dependence on material properties other than stress makes use of the Barkhausen technique highly material and component geometry specific.

Calibration of the Barkhausen probe is necessary to account for the effect that hardness, texture, grain size, and other material properties have in the presence of a varying residual stress field. In the case of pipe, a calibration tool can be made using a section of the pipe instrumented with electrical resistance strain gauges to provide a means of measuring the MP as a function of applied stress. In the case of welds, where there is a wide range of grain size, hardness, and even composition within the weld HAZ, none of the nonstress properties can be assumed to be constant, and interpretation of the Barkhausen data must be used with caution. Rapid detection of potential zones of tension may be then confirmed by other residual stress measurement techniques such as XRD or hole drilling.

The Barkhausen magnetic method can be summarized as (i) being suitable for only ferromagnetic materials, (ii) limited to measuring surface layers of the material, (iii) limited in measurement range by saturation of the Barkhausen noise response when testing compressive residual stresses, particularly in hard steels, and (iv) sensitive to a variety of microstructural variations (grain size, hardness, and texture),

making separation of those contributions from stresses difficult [32].

7.4 CONTROL AND ALTERATION OF RESIDUAL STRESSES

The engineer has a variety of tools for modifying the residual stresses that are encountered to reduce or eliminate the adverse effects of tensile residual stress. Machining and grinding practices can be modified to avoid surface tension. Weld shrinkage-induced tension can be reduced by well-established practices of preheating or postweld thermal stress relief. However, it is also possible to introduce beneficial residual compression using surface enhancement methods to further improve performance beyond that achievable with the available materials, even in a stress-free state. When material substitution is not an option, and applied stresses cannot be reduced, surface enhancement can ensure reliable performance, especially in highly stressed critical locations. Several of the available surface enhancement methods are briefly described.

7.4.1 Shot Peening

Shot peening is the most widely used surface enhancement method. Metallic or ceramic shot, ranging in size from nominally 0.25 mm (0.010 in.) to as large as 3.18 mm (0.125 in.), impacts the surface of the component, producing spherical indentations. The shot peening process forms a compressive layer through a combination of subsurface compression developed by Hertzian loading combined with lateral displacement of the surface material around each of the dimples. As the dimples overlap with random impacts, the entire surface is effectively elongated, driving the surface layer of deformed material into compression as its expansion is resisted and supported by the equilibrating tension in the material below.

Metallic shot is often either cast steel or cut wire blasted against a carbide plate to form a nearly spherical shape. Cut wire shot can be manufactured from virtually any alloy to avoid elemental contamination. Ceramic shot is typically zirconium oxide or glass bead. The shot will wear and fracture during use; therefore, the shot peening media should be constantly screened to remove broken shot and dust.

The shot peening process is defined by parameters that include the size and type of shot used, the Almen intensity achieved, and the coverage. Almen intensity is a measure of the deflection of the Almen A, C, or N strip that occurs during the peening cycle, and is a measure of the elastic energy stored in the 1070 steel Almen strip by the formation of a layer of residual compression. Almen intensity is only a process control tool. The Almen strip arc height is related to the area under the residual stress depth curve in the Almen

strip, and it does not uniquely define a depth or magnitude of compression in either the strip or the component being shot peened. Coverage is the percentage of the surface impacted by shot, and is a function of time under the shot stream. In order to ensure uniform treatment of the surface, coverage is often specified at 100% or higher, implying that each point on the surface was impacted at least one or more times.

The shot is accelerated to sufficient velocity to deform the surface on impact, either by air blast or wheel machines. In wheel shot peening machines, the shot is thrown from a rapidly spinning radially bladed wheel. Air blast machines propel the shot in a stream of compressed air through a hardened carbide nozzle. Flapper peening is a form of controlled shot peening without free flying shot. The flapper tool has captive shot embedded, like rivets, in rubberized fabric flaps that are attached radially to rotate around a shaft. The shaft is rotated so that the flaps successively impact the surface peening of a local area. Flapper peening is used for repair or limited access work or when free shot cannot be tolerated, as in field-welded joints in pipelines [34].

By its very nature, shot peening relies upon random impacts of shot. In order to achieve the coverage requirements, some regions will receive numerous impacts before adjacent areas are impacted at all. The result is a nonuniform and often very highly cold-worked surface, especially for high coverage peening. Cold work levels range from 40% to over 100% during creation of the layer of surface compression. In the work hardening materials, such as austenitic alloys, peening-induced cold working can exhaust the ductility of the material, leaving a brittle surface layer. Shot peening damage in the form of “laps and folds” creates stress concentrations that reduce fatigue performance.

Shot peening is a very practical surface enhancement method, provided the components are not exposed to elevated temperatures or mechanical overload. Research has shown that the highly cold-worked shot-peened surface will relax more completely and much faster than a low cold-worked surface at the same state of compressive stress [18].

7.4.2 Roller or Ball Burnishing and Low Plasticity Burnishing

In roller or ball burnishing, a wheel-like axle-mounted roller or a hydrostatically supported ball is pressed against the surface. The tool is then moved over the surface, repeatedly deforming the surface layer to create compression up to nominally 1 mm, or more, deep. Like shot peening, the compressive residual stress creating mechanism is a combination of subsurface yielding by Hertzian loading and lateral displacement of the surface material. Conventional roller burnishing deliberately creates a highly cold-worked layer that is also in high residual compression. Roller burnishing is generally performed in lathe operations, advancing the tool with each revolution at a constant feed rate.

LPB differs from conventional roller and ball burnishing primarily by imparting the minimal amount of cold working needed to create the depth and magnitude of residual compression required to achieve the desired damage tolerance and fatigue or stress corrosion performance. Low cold work provides both thermal and mechanical stability of the beneficial compression. LPB uses a constant volume hydrostatic tool design to “float” the burnishing ball continuously during operation, regardless of the force applied, to avoid damaging the surface. The LPB burnishing force can be optimized for each application and varied under closed-loop control to impart the depth and magnitude of compression required in just the critical failure-prone locations. By controlling the burnishing force, LPB produces a depth of compression ranging from a few thousandths of an inch to over a full centimeter under closed-loop control.

7.4.3 Laser Shock Peening

The laser shock peening process introduces compression with low cold working using shock waves to yield the material. Laser peening utilizes high-speed, high-powered lasers to focus a short-duration energy pulse on a coating, usually black tape, on the surface of the work piece to absorb the energy of the laser beam. A transparent layer of flowing water covers the tape to direct the shock wave energy into the surface of the material. When the laser is fired periodically, the laser beam passes through the water, explodes the tape, and creates a shock wave sufficient to deform the material to depths typically on the order of a millimeter. The shocking process is repeated in a computer-controlled pattern across the surface, creating a series of slight indentations and regions of residual compression. Several cycles or “layers” of peening are often required. Although limited by cost, quality control, and logistical issues, laser peening has been studied as a means of introducing residual compression in pipelines and the residual stress distributions documented [35].

Figure 7.14 shows subsurface stress profiles for each surface treatment process and the cold work induced in titanium.

7.4.4 Thermal Stress Relief

Thermal stress relief is widely used to reduce residual stresses. Postweld heat treatment of pipeline joints reduces the detrimental tensile stresses generated by welding. The reader is referred to the API bulletin 939E for a detailed discussion of procedures for postweld heat treatment of pipe sections.

The primary process at work in thermal stress relaxation is a creep mechanism. Residual stresses relax exponentially with both time and temperature, reducing the overall strain energy. Both tensile and compressive residual stresses are reduced as the temperature of the material is increased. No stresses higher than the yield strength at the maximum

exposure temperature can be retained in the component. The conventional rule of thumb for thermal stress relief of steels based upon this time–temperature relaxation mechanism is exposure to 611 °C (1150 F) for a period of 1 h for each 25 mm (1 in.) of thickness, with the minimum of 1 h for any thickness being stress relieved.

Another mechanism more recently recognized is the rapid relaxation of residual stress in a highly cold-worked material [36]. At elevated temperatures, the deformed surface of machined, ground, shot-peened, and other surfaces that have high dislocation density can relax virtually immediately by a dislocation annihilation mechanism, which is then followed by the slow exponential relaxation. This effect can cause a loss of beneficial compression from shot peening with elevated temperature exposure, particularly in austenitic alloys.

Residual stresses do not relax uniformly, that is, not in proportion to the original levels present at each point in the body, because the amount and rate of stress relaxation depend upon the initial stress magnitude. Furthermore, the residual stress distribution will re-equilibrate as the regions of higher tension or compression relax more rapidly, and by a greater amount, than the lower stress regions. Stresses may actually increase in some areas following thermal stress relief as more highly stressed regions relax and the body re-equilibrates. Because the rate of relaxation depends upon the stress level, complete thermal stress relief is nearly impossible to achieve. Once the stresses are reduced, the driving force for further relaxation diminishes, and some level of stress is invariably retained.

Successful thermal stress relief requires uniform temperature throughout the component during the process. If there are large thermal strains created during either the heating or the cooling stages of the thermal cycle, the plastic strains introduced at the temperature can result in even higher residual stresses after cooling than were present before heating. Quenching from elevated temperatures is an extreme case of high thermal strain, and the source of residual “quench stresses.” Complex geometries such as heat exchangers require very slow heating and cooling. It may be impossible to thermally stress relieve components composed of dissimilar materials with different coefficients of thermal expansion. The key to a successful thermal stress relief is to keep the entire body at a nominally uniform temperature, which is slowly raised to the critical temperature, held for the required exposure time, and then cooled back to ambient temperature without creating thermal strains that could cause plastic deformation.

7.5 CASE STUDIES OF THE EFFECT OF RESIDUAL STRESS AND COLD WORK

Thermal stress relaxation can only reduce the magnitude of undesirable residual stresses, but cannot introduce beneficial

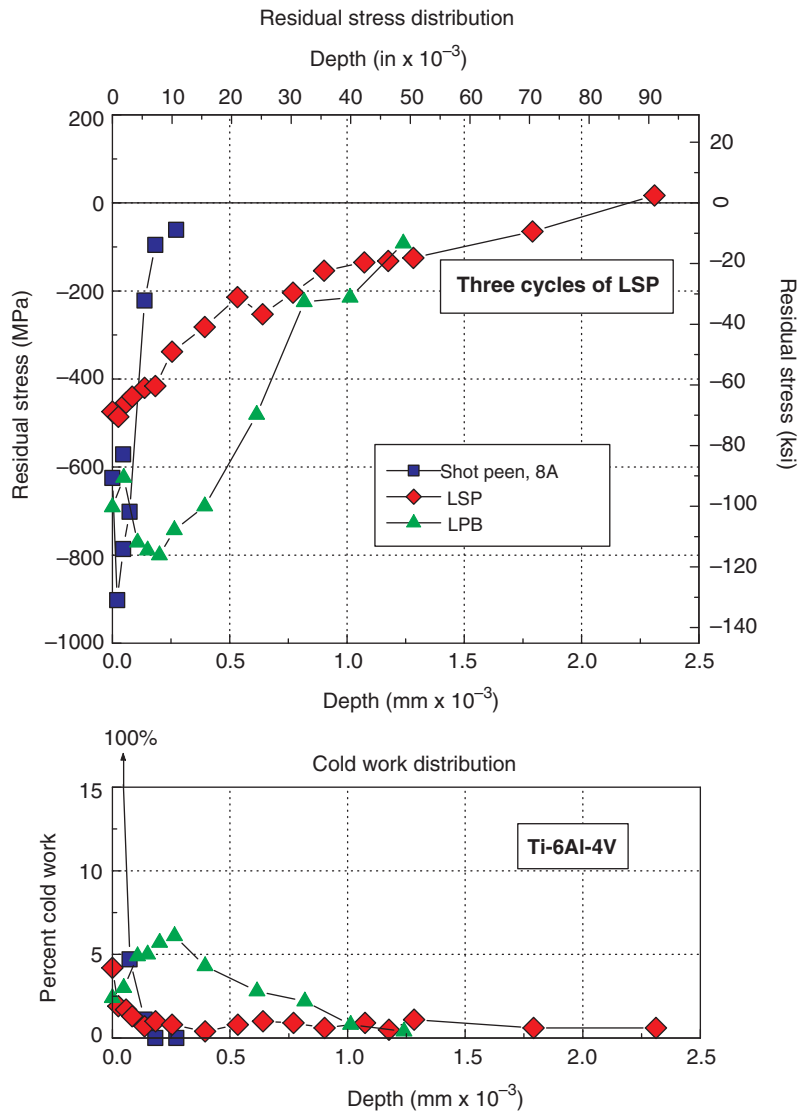


FIGURE 7.14 Stress profiles and cold work from SP, LPB, and LSP.

compression to advantage. It must also generally be applied to all or large portions of a component to avoid creating large thermal strains. Mechanical surface enhancement treatments introduce beneficial compressive residual stress to critical locations to eliminate detrimental tension or improve performance at the high-stress critical locations. The following case studies provide examples of use of surface enhancement to mitigate SCC and improve fatigue performance in pipeline-related applications.

7.5.1 Case Study 1: Restoration of the Fatigue Performance of Corrosion and Fretting Damaged 4340 Steel

Corrosion pits commonly form at the site of inclusions on the material surface. Pits can be rounded or branched as the pit

grows into the surface, and form fatigue crack initiating stress concentrations. Corrosion pitting damage generally increases with time. The fatigue debit from pitting is typically on the order of half of the endurance limit of the material. The fatigue strength can be restored by introducing a layer of compressive residual stress that is deeper than the corrosion pits to prevent fatigue crack growth from the bottom of the pits.

The effect of introducing compressive residual stress on fatigue performance was studied for 4340 steel with corrosion pitting in a salt fog chamber [37]. The benefits of surface enhancement were investigated with fatigue tests conducted in four-point bending at a stress ratio $S_{min}/S_{max} = 0.1$ after exposure to salt fog for 100 and 500 h. Samples were tested with and without wire brushing to remove the corrosion product, as might be performed during maintenance.

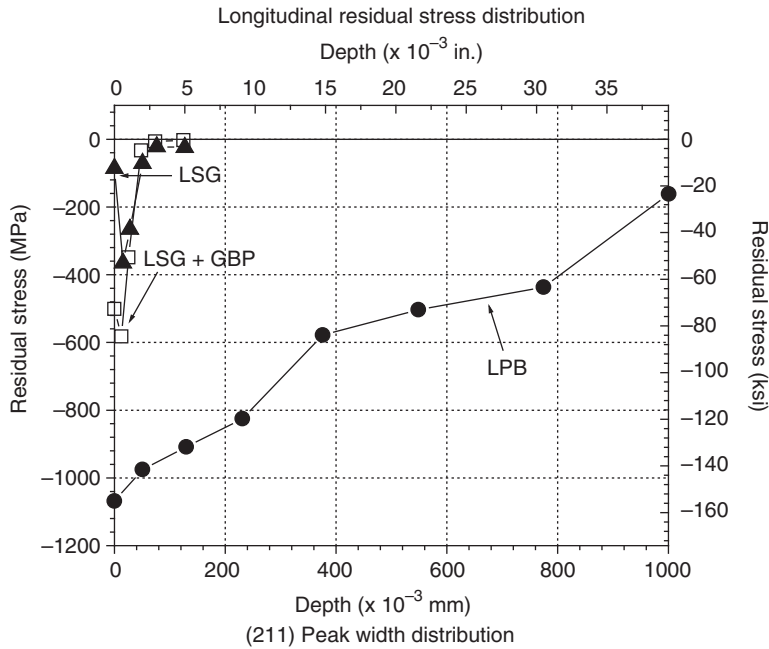


FIGURE 7.15 Subsurface residual stress distributions of LSG, GBP, and LPB 4340 steel.

Residual stress distributions measured by X-ray diffraction are shown in Figure 7.15. Surfaces were low-stress ground (LSG), glass bead peened (GBP), and LPB. LSG is the common baseline condition for fatigue sample preparation, producing shallow compression typical of cold abrasion processes. GBP produced an equally shallow (0.05 mm) layer of higher -600 MPa magnitude. LPB produced a layer

of compression over 1 mm deep starting at over -1000 MPa on the surface.

The fatigue results in Figure 7.16 show that pitting from 100 and 500 h salt fog exposures reduced the 10^7 cycle fatigue strength by nominally 25 and 50%, respectively. Fatigue cracks initiated in corrosion pits in all cases. LPB applied to the corroded surfaces after superficial cleaning to

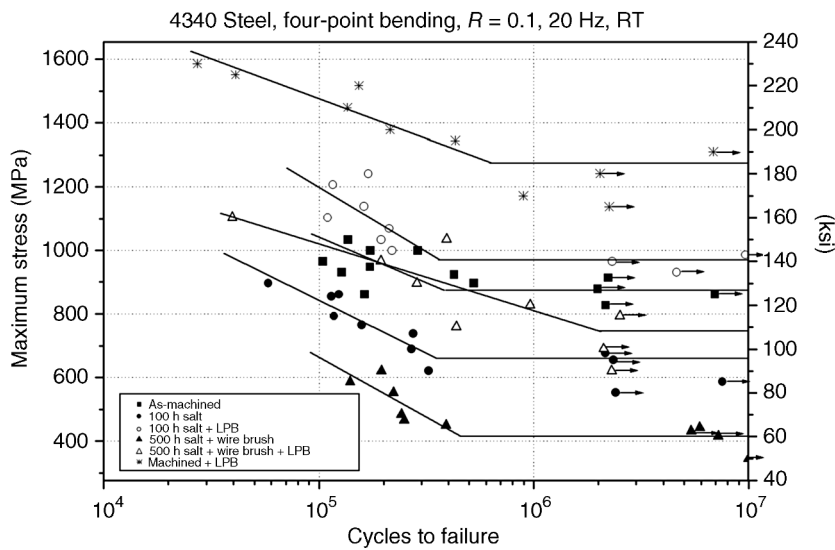


FIGURE 7.16 High cycle fatigue S/N data.

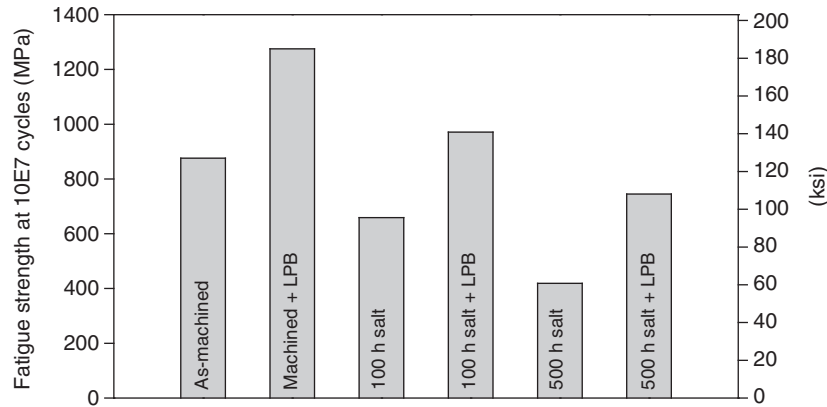


FIGURE 7.17 Long-life fatigue strength (4340 steel).

remove loose corrosion product restored the fatigue strength to 110% of the original strength after 100h exposure and 85% after 500h. The relative fatigue strength at 10^7 cycles, summarized in Figure 7.17, is attributed to the increased depth of pitting with exposure time.

Fretting damage causes fatigue failures in components that are clamped together and vibrate, such as bolted flange joints in pipelines. The combination of clamping stress pressing the surfaces together and alternating normal stresses in the plane of the surface produces high shear stresses at the edges of contact that initiate shear cracks. The shear stresses are high only at the surface, and the shear cracks produced are generally limited to depths of less than 0.08 mm (0.003 in.). The shallow shear cracks ultimately propagate in fatigue to

failure driven by the alternating normal stresses. The fatigue debit from fretting is typically on the order of half of the endurance limit of the material, but can be mitigated by arresting fatigue crack propagation with a layer of residual compressive stress deeper than the maximum depth of the shear cracks.

A “bridge” fretting fatigue apparatus [38] was used with flat samples loaded in four-point bending to study the effect of surface treatments on 4340 steel, 50 HRC, before, after, and with repeated fretting damage. The multiple fretting exposures were intended to simulate combinations of damage in service, overhaul with treatment, and return to service. Figure 7.18 shows the results of a study of GBP and LPB, with fretting damage either before or after surface enhancement.

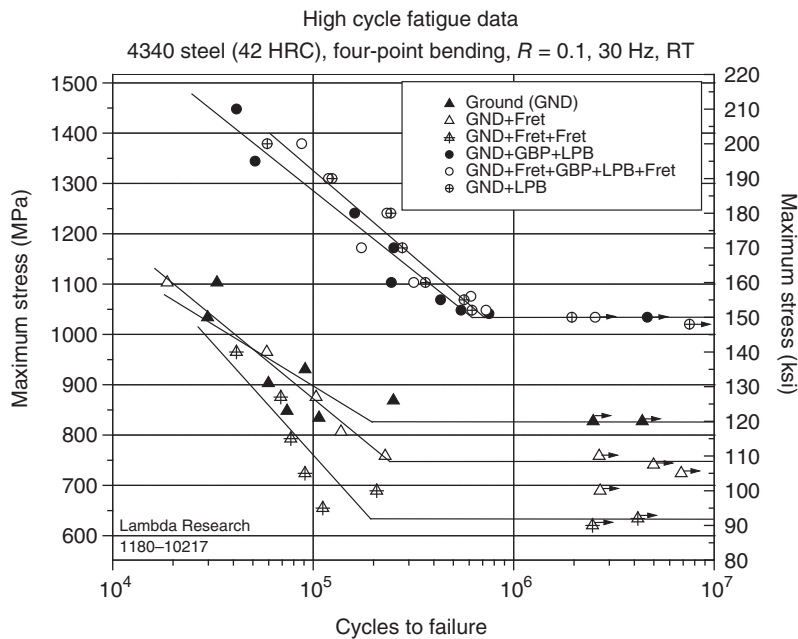


FIGURE 7.18 4340 Steel fretting fatigue results, as ground and with prior LPB treatment.

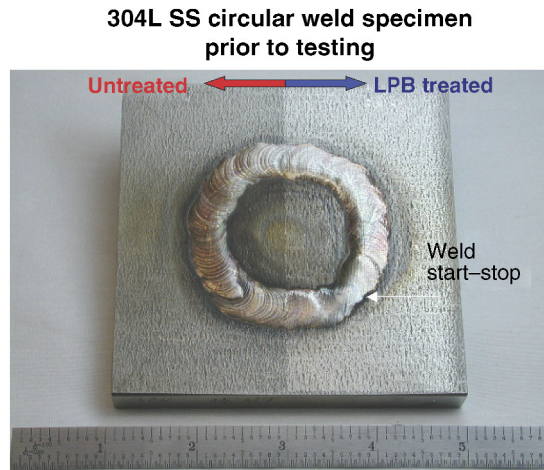


FIGURE 7.19 304L SS butt-welded plate specimen, half LPB processed.

The fretting fatigue debit was entirely eliminated with a layer of compression deeper than the fretting damage, and surface enhancement increased the HCF strength 25% over the baseline ground condition.

7.5.2 Case Study 2: Mitigating SCC in Stainless Steel Weldments [39]

SCC can occur only in a susceptible alloy where the net tensile stress (residual and applied) exceeds a threshold level in a corrosive environment. Austenitic stainless steels, including 304L and 316L, are SCC-susceptible alloys, especially in the “sensitized” condition. Sensitization occurs in the HAZ of welds that have reached a temperature at which Cr can precipitate out of solution forming carbide inclusions along the grain boundaries. Because the sensitization temperature is nominally the same as that required for thermal stress relaxation, thermal stress relief of these welds generally is not possible. If the SCC environment cannot be avoided, and thermal stress relief is not practical, the net stress level can be reduced to less than the SCC threshold by introducing a layer of residual compression into the surface.

Two different symmetrical weld geometries were prepared and processed using LPB to produce a 1 mm depth of compressive residual stress on half of each specimen. The samples were a circular weld deposit and a butt-welded pipe, as shown in Figures 7.19 and 7.20.

Residual stresses produced by welding were first measured by X-ray diffraction as functions of distance and depth on the untreated and treated sides of the 316L circular welded plate. Figure 7.21 shows compressive residual stresses within the treated zone and tensile stresses from weld contraction within the untreated zone, extending to beyond the measured maximum depth of 0.50 mm (0.020 in.).

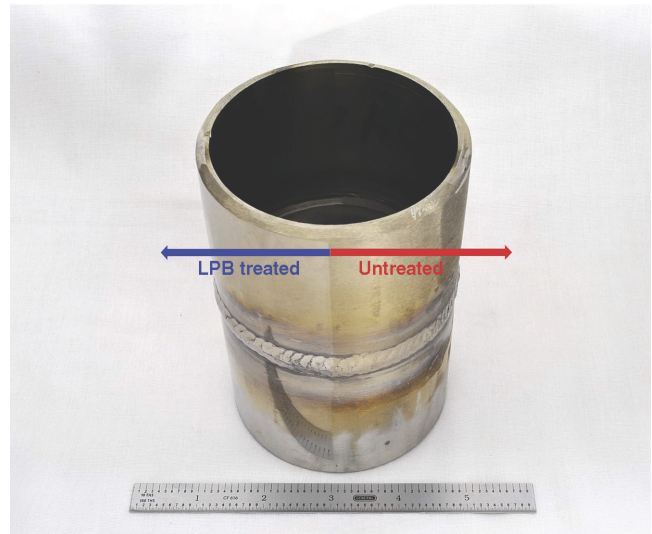


FIGURE 7.20 316L SS circular welded plate specimen, half LPB processed.

The effectiveness of SCC mitigation was aggressively tested in heated $MgCl_2$ solution, followed by dye penetrant inspection. The untreated welds suffered severe SCC damage due to the combination of residual tension from the welding operation and sensitization during the welding heat cycle. The fluorescent dye penetrant examination photos in Figure 7.22 reveal complete mitigation of SCC by the deep compressive residual stress layer. Propagating cracks are arrested at the boundary of the treated half.

The sectional view in Figure 7.23 reveals that the cracks penetrated entirely through the 12.5 mm (0.5 in.) thick welded plate. Cracks originating in the untreated half of the circular weld samples and propagating entirely through the thickness were arrested without penetrating under the compressive layer of the treated material.

The 304L butt-welded pipe sections showed the same behavior as the circular welds. Florescent dye penetrant inspection shown in Figure 7.24 revealed that no SCC occurred on the compressive surface of the treated side.

Introduction of beneficial compression to eliminate residual tension in critical locations, such as sensitized austenitic stainless steel welds, can dramatically improve resistance to SCC.

7.5.3 Case Study 3: Mitigation of Sulfide Stress Cracking in P110 Oil Field Couplings [40]

Another form of SCC, sulfide stress cracking and hydrogen embrittlement (HE), limits the use of high-strength carbon steels in H_2S -containing “sour” service environments. High-magnitude tensile stresses are generated in threaded connections during power makeup of downhole tubular components. These coupling stresses can be considered to be

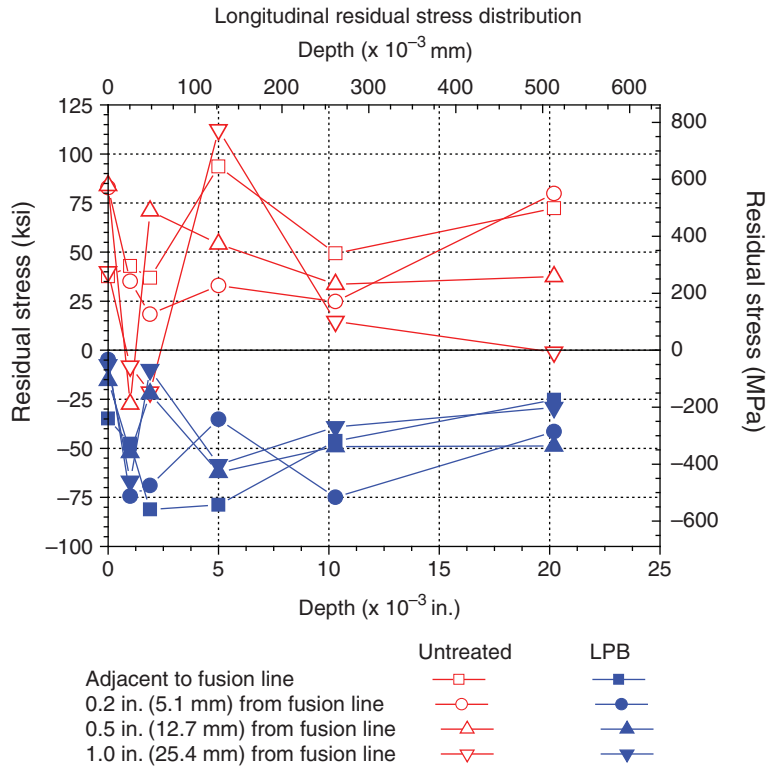


FIGURE 7.21 Longitudinal residual stress versus depth on a 316L circular welded plate. Compression extends over 25 mm (1.0 in.) through the fusion line and HAZ.

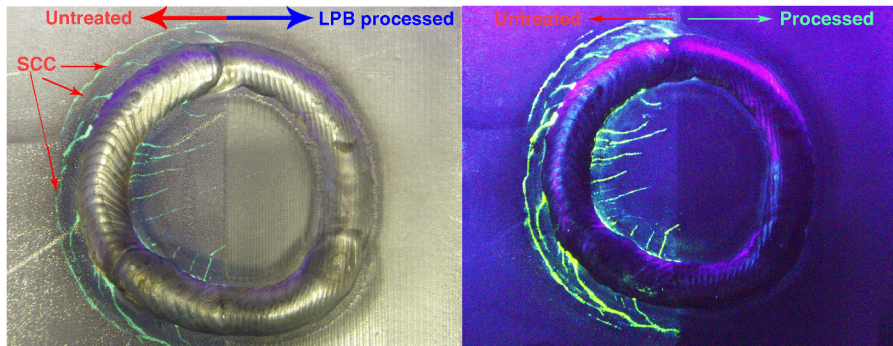


FIGURE 7.22 Fluorescent dye penetrant reveals severe SCC on 304L circular weld specimen (ambient and UV lighting).

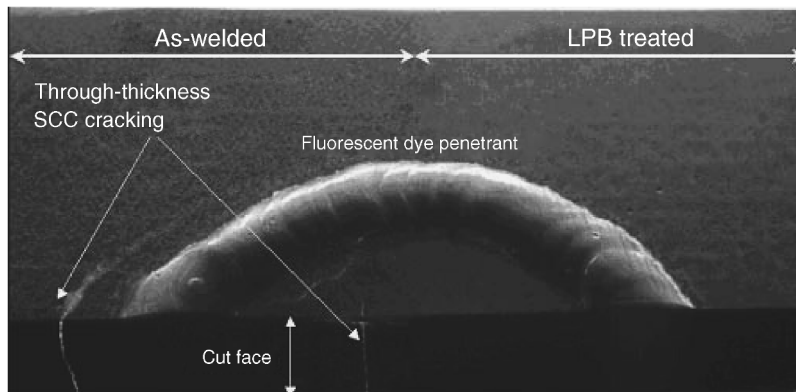


FIGURE 7.23 Fluorescent dye penetrant photo showing through-thickness SCC cracking on untreated side of 304L SS circular weld specimen.

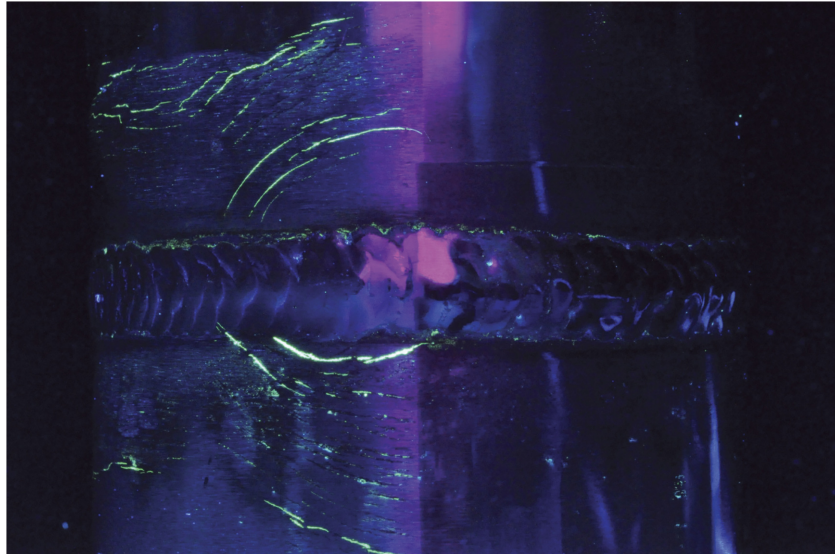


FIGURE 7.24 SCC on untreated side of 304L SS pipe weld specimen (left). Fluorescent dye shows no cracking on the LPB-processed regions.

“residual” fit-up stresses once the connections are made and placed in service. Service loads can then increase the total stress to exceed the threshold tensile stress for SSC initiation. High-strength steel grades are generally preferred, but have inherently lower K_{ISCC} , and are at higher risk of SSC in sour service than the low-strength grades. The conventional options are to use more expensive SSC-resistant alloys or to accept the strength limitations of lower strength grades to reduce the chance of SSC failure.

Introduction of stable, high-magnitude compressive residual stresses into less-expensive carbon steel alloys alleviates the tensile stresses and mitigates SSC, while also improving fatigue strength. Less-expensive alloys could then be used in sour environments. The benefits of introducing a 1 mm deep layer of high compression on SSC performance were evaluated in C-ring specimens and on full-size pressurized quench and tempered API P110 steel coupling blanks with a yield strength of 910 MPa (132 ksi). The C-ring and the full-size 4.5 in. coupling blanks specimens are shown in Figure 7.25.

Both specimen types were statically loaded to fixed fractions of the specified minimum yield stress (SMYS) and exposed to 100% NACE TM0177 H₂S solution A. No SSC failures occurred in LPB-treated test specimens

stressed up to 85% SMYS hoop tension, exceeding the NACE 720 h exposure requirement.

Figure 7.26 shows that untreated coupling blanks failed in 37.5 h at 45% SMYS, but treated couplings run out the 720 h test duration even at 95% SMYS. The C-ring sample results, shown in Figure 7.27, were comparable. Untreated, baseline samples failed in 10 h at 45% SMYS. Treated samples exceeded 840 h exposures stressed at 90% SMYS.

The SSC results confirm that the compressive residual stress layer at 1 mm deep isolated the material from the corrosive H₂S environment and eliminated sour well cracking. As observed for the welded stainless steel in chloride SCC, the total stress in the compressive surface layer remains below the threshold for SSC even under applied service stresses up to the yield strength of the alloy. Surface enhancement mitigates H₂S cracking allowing high-strength steel to be used in an otherwise prohibitive environment.

7.5.4 Case Study 4: Improving Corrosion Fatigue Performance and Damage Tolerance of 410 Stainless Steel [41]

CF and SCC occur in ferritic and martensitic stainless steel components. Shot peening is widely used to improve fatigue

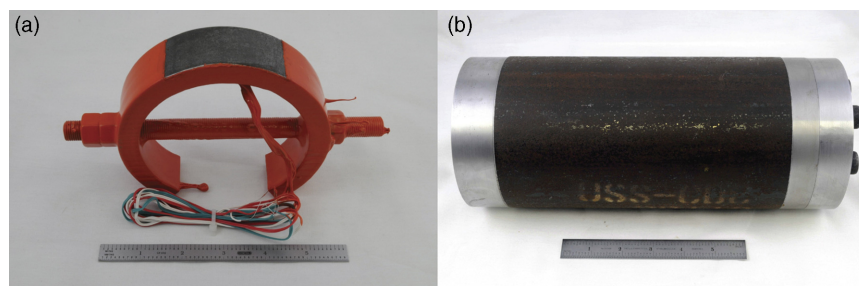


FIGURE 7.25 (a) C-ring specimen and (b) full-sized coupling blank in test fixture.

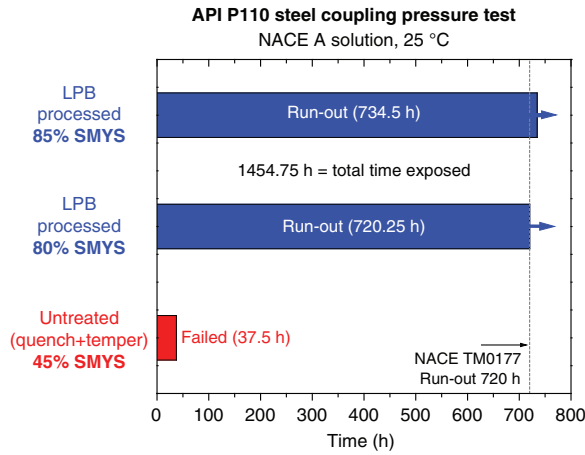


FIGURE 7.26 Full-sized P110 coupling blank pressure test results (in NACE A solution).

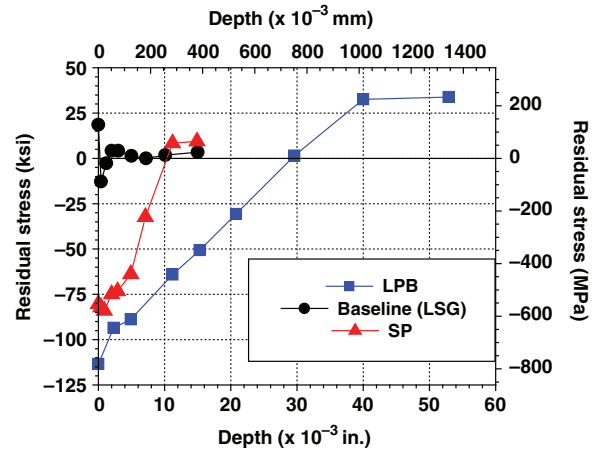


FIGURE 7.28 Residual stress profiles for low plasticity burnishing, low stress grinding, and shot peening.

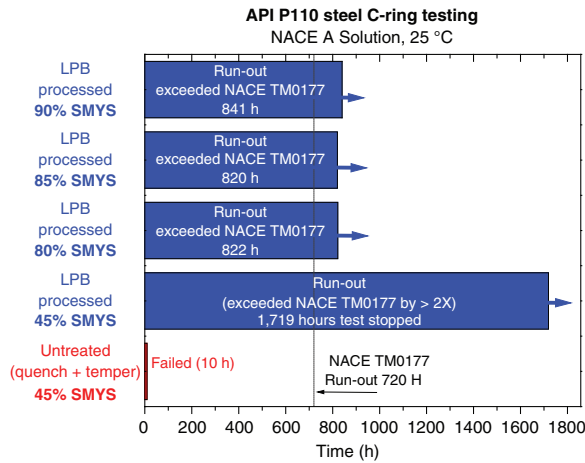


FIGURE 7.27 P110 C-ring test results (in NACE A solution).

performance; however, the repeated random impacts from SP can produce a highly cold-worked surface. Corrosion pits or mechanical damage can penetrate the relatively shallow SP compressive layer, providing initiation sites for SCC and CF. Low plasticity burnishing produces deeper compression with lower cold working of the surface. Residual stress distributions obtained using X-ray diffraction are plotted as a function of depth in Figure 7.28 for samples processed using SP, LPB, and LSG used for fatigue sample preparation.

High cycle fatigue tests were conducted on type 410 stainless steel to determine the benefits of LPB and SP in mitigating surface damage by introducing notches to simulate foreign object damage, pitting damage, or erosion prior to testing. The effects of 0.25 and 0.50 mm (0.01 and 0.02 in.) mechanical damage on fatigue life are shown in Figure 7.29. Because the residual compression from LPB was deeper than the damage in the samples, LPB provided nominally a 100× improvement in fatigue life compared with the shallow compression from SP.

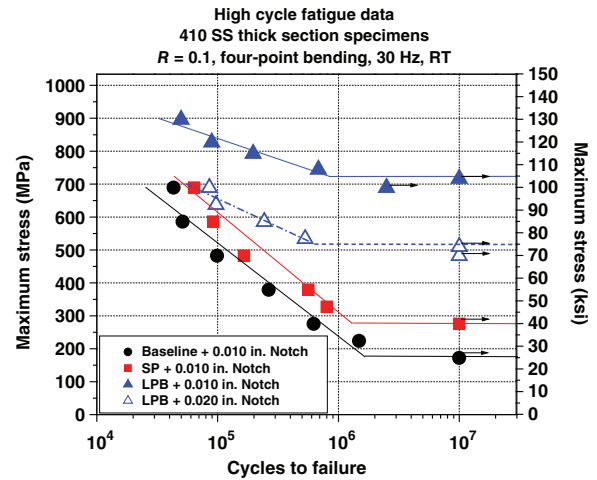


FIGURE 7.29 High cycle fatigue results for 410 SS with mechanical damage.

High cycle corrosion fatigue tests were conducted in an active corrosion (AC) medium of 3.5% weight NaCl solution on type 410 stainless steel to determine the effect of LPB and SP on corrosion fatigue performance. The S–N curves for samples subject to prior SCC damage and fatigue tested in active corrosion are shown in Figure 7.30. Baseline and SP samples have similar fatigue performance. Prefatigue SCC damage with active corrosion during fatigue introduces a fatigue debit of 50% of the endurance limit. The debit from corrosion was nearly as high as that resulting from the 0.25 mm (0.01 in.) deep notch. LPB-treated samples have nominally twice the fatigue strength of the baseline and SP samples and an increase in life nominally 50× that of the SP or baseline conditions.

The cold work associated with the surface treatments can adversely affect the corrosion behavior. Polarization curves for LPB- and SP-treated samples are shown in Figure 7.31.

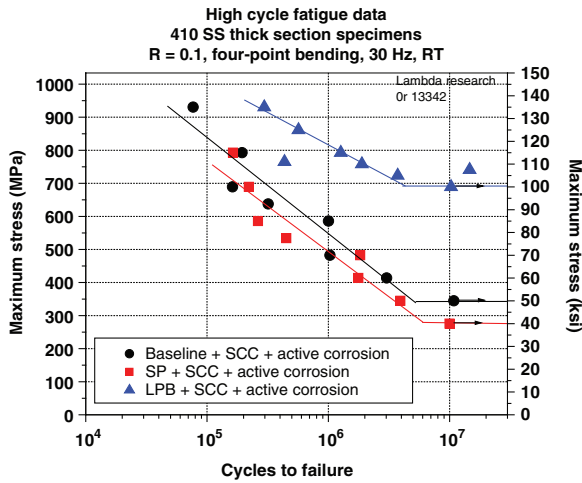


FIGURE 7.30 High cycle fatigue results for specimens with SCC and active corrosion.

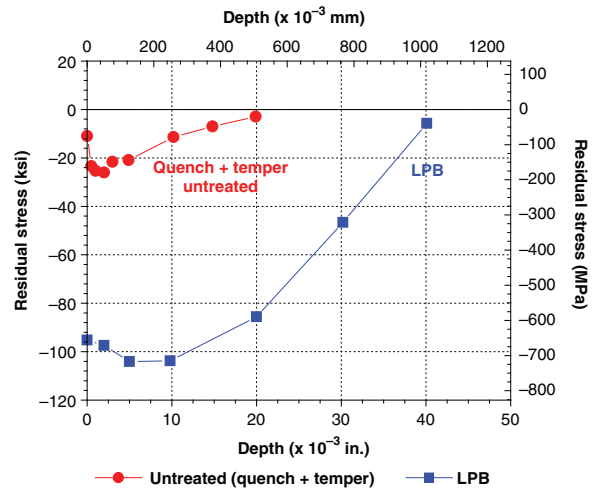


FIGURE 7.32 Residual stress distribution for as-received and LPB-processed API-P110 couplings.

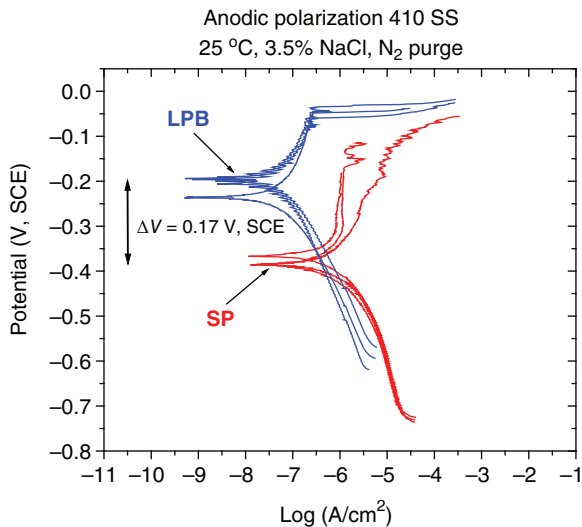


FIGURE 7.31 Anodic polarization curves for shot-peened and LPB-treated 410 SS.

The shift in the OCP indicates greater electrochemical activity and susceptibility to corrosion at the surface of the more highly cold-worked SP surface. Tafel slope extrapolations of the curves yield a corrosion rate of 14.7 mm per year (0.58 mils per year) for the SP surface, and 0.8 mm per year (0.03 mils per year) for LPB. The SP surface is corroding at 20× the corrosion rate of the lower cold-worked LPB surface.

7.5.5 Case Study 5: Improving the Fatigue Performance of Downhole Tubular Components [42]

The P110 couplings used in horizontal drilling are subjected to high bending stresses and high internal pressures, especially in fracking operations. Fatigue failure exacerbated by

mechanical damage and corrosive environments, such as H₂S and NaCl, is a major problem in these downhole tubular components. Surface enhancement introduces a layer of beneficial compressive residual stress to alleviate applied tensile stresses and mitigate damage and SCC to improve fatigue performance.

Quench and tempered API P110 grade steel couplings were LPB treated on the OD for surface enhancement. Residual stress measurement by X-ray diffraction shown in Figure 7.32 revealed compression of -700 MPa (-100 ksi) extending 1 mm into the surface after treatment.

Untreated and LPB-treated P110 samples were tested with mechanical damage or corrosive damage at ambient temperature in four-point bending at 30 Hz and stress ratio $S_{min}/S_{max}=0.1$. Active corrosion fatigue testing was performed in a neutral 3.5 wt.% NaCl solution. Several fatigue samples were given prior to SCC exposure in NaCl solution to simulate extended service exposure.

Figure 7.33 shows fatigue results as stress versus life (S-N) curves. The 10⁷ cycle fatigue strength of as-machined, baseline, P110 with 0.5 mm (0.020 in.) deep mechanical damage is only 170 MPa (25 ksi), compared with 345 MPa (50 ksi) with LPB. Surface enhancement provided nominally 2× the fatigue strength and a 50× increase in life, even with fatigue initiating surface damage present. Corrosion damage reduced the fatigue strength of untreated P110 to less than 138 MPa (20 ksi). P110 pipe after LPB in active corrosion fatigue has 1.75× greater fatigue strength of 241 MPa (35 ksi), and nominally an order of magnitude increase in life.

Polarization testing conducted on low cold-worked (electropolished) and high cold-worked (shot-peened) P110 steel test samples is shown in Figure 7.34. The shift in OCP indicates greater electrochemical activity and susceptibility to corrosion at the surface of the highly cold-worked shot-peened surface.

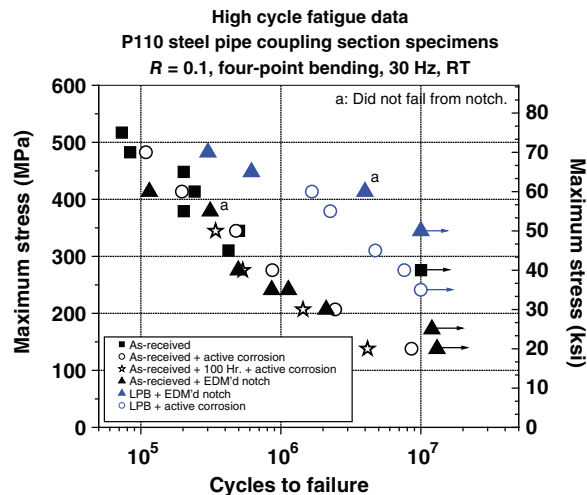


FIGURE 7.33 High cycle fatigue results for API-P110 steel specimens with damage and corrosion.

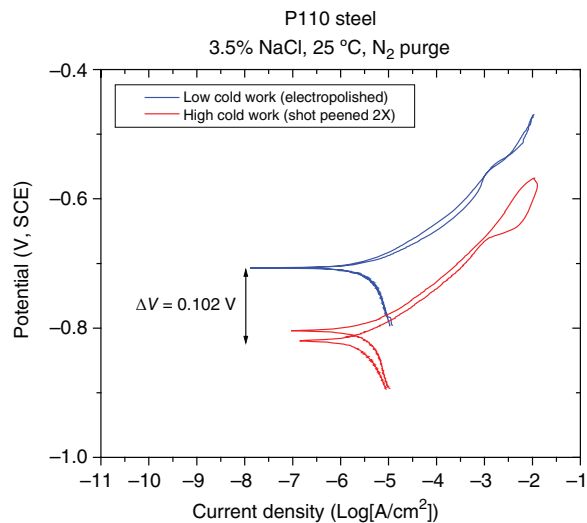


FIGURE 7.34 Anodic polarization curves low cold-work and shot-peened P110 steel.

REFERENCES

- Walker, T.R. and Pick, R.J. (1990) Approximation of the axial strains developed during the roll forming of ERW pipe. *Journal of Materials Processing Technology*, 22(1), 29–44.
- Weng, C.C. and Pekoz, T. (1990) Residual stresses in cold-formed steel members. *Journal of Structural Engineering*, 116(6), 1611–1625.
- Scaramangas, A. and Goff, P.R. (1985) Residual stresses in cylinder girth butt welds. Offshore Technology Conference.
- Bate, S.K., Green, D., and Buttle, D. (1997) *A Review of Residual Stress Distributions in Welded Joints for the Defect Assessment of Offshore Structures*, HSE Books.
- Brinksmeier, E., Cammett, J.T., Konig, W., Leskovar, P., Peters, J., and Tonshoff, H.K. (1982) Residual stresses:

measurements and causes in machining processes. *CIRP Annals: Manufacturing Technology*, 31(2), 491–510.

- Antaki, G.A. (2003) *Piping and Pipeline Engineering: Design Construction, Maintenance, Integrity and Repair*, CRC Press, Vol. 159, pp. 411–412.
- Shi, Y.W., Chen, B.Y., and Zhang, J.X. (1990) Effects of welding residual stresses on fatigue crack growth behaviour in butt welds of a pipeline steel. *Engineering Fracture Mechanics*, 36(6), 893–902.
- Jayaraman, N. and Prevey, P. (2007) A design methodology to take credit for residual stresses in fatigue limited designs. *Residual Stress Effects on Fatigue and Fracture Testing*, STP1497, American Society for Testing and Materials, Lancaster, PA, pp. 69–84.
- Snape, E. (1967) Sulfide stress corrosion of some medium and low alloy steels. *Corrosion*, 23(6), 154–172.
- Makarenko, V.D. and Khalin, A.N. (2005) Effects of hydrogen on the corrosion failure of welded pipelines. *Chemical and Petroleum Engineering*, 41(7–8), 448–450.
- Ghosh, S., Rana, V.P.S., Kain, V., Mittal, V., and Baveja, S.K. (2011) Role of residual stresses induced by industrial fabrication on stress corrosion cracking susceptibility of austenitic stainless steel. *Materials and Design*, 32(7), 3823–3831.
- Beavers, J. (2010) Recent progress in understanding and mitigating SCC of ethanol pipelines. Corrosion 2010, NACE International, Houston, TX.
- Chandra, U. (1985) Determination of residual stresses due to girth-butt welds in pipes. *Journal of Pressure Vessel Technology*, 107(2), 178–184.
- Brust, F.W. and Kanninen, M.F. (1981) Analysis of residual stresses in girth welded type 304 stainless steel pipes. *Journal of Materials for Energy Systems*, 3(3), 56–62.
- Chen, W., Van Boven, G., and Rogge, R. (2007) The role of residual stress in neutral pH stress corrosion cracking of pipeline steels—Part II: crack dormancy. *Acta Materialia*, 55(1), 43–53.
- Huang, H. and Shaw, W.J.D. (1992) Electrochemical aspects of cold work effect on corrosion of mild steel in sour gas environments. *Corrosion*, 48(11), 931–939.
- Huang, H. and Shaw, W.J.D. (1993) Cold work effects on sulfide stress cracking of pipeline steel exposed to sour environments. *Corrosion Science*, 34(1), 61–78.
- Prevey, P.S. (2000) The effect of cold work on the thermal stability of residual compression in surface enhanced IN718. 20th ASM Materials Solutions Conference & Exposition, ASM, St. Louis, MO, pp. 426–434.
- Lu, J. (editor) and Society for Experimental Mechanics, Inc. (1996) *Handbook of Measurement of Residual Stresses*, Fairmont Press, Inc., Lilburn, GA.
- Schajer, G. (editor) (2013) *Practical Residual Stress Measurement Methods*, John Wiley & Sons, Inc., New York
- Zeinoddini, M. (2013) Repair welding influence on offshore pipeline residual stress fields: an experimental study. *Journal of Constructional Steel Research*, 86, 31–41.

22. Lu, J. (editor) and Society for Experimental Mechanics, Inc. (1996) Magnetic methods. *Handbook of Measurement of Residual Stresses*, Fairmont Press, Inc., Lilburn, GA.
23. ASTM (2008) ASTM E837: Standard Test Method for Determining Residual Stresses by the Hole-Drilling Strain-Gage Method. American Society for Testing and Materials.
24. Vishay Precision Group (2010) Measurement of residual stresses by the hole-drilling strain gage method. Micro-Measurements Tech Note T-503-6.
25. Keil, S. (1992) Experimental determination of the residual stresses with the ring-core method and an on-line measuring system. *Experimental Techniques*, 16(5), 17–24.
26. Lu, J. (editor) and Society for Experimental Mechanics, Inc. (1996) *Handbook of Measurement of Residual Stresses*, The Fairmont Press, Inc., Lilburn, GA.
27. Hornbach, D. (2009) Incremental ring-core determination of the principal residual stress in a duplex stainless steel centrifuge. Lambda Research, Diffraction Notes 35.
28. SAE (2003) Residual Stress Measurement by X-ray Diffraction. SAE HS784, Society of Automotive Engineers.
29. ASTM (1984) *Standard Method for Verifying the Alignment of X-Ray Diffraction Instrumentation for Residual Stress Measurement*. ASTM E915-10, Vol. 03.01, American Society for Testing and Materials, Philadelphia, PA, pp. 809–812.
30. ASTM (2009) Standard Test Method for Determining the Effective Elastic Parameter for X-Ray Diffraction Measurements of Residual Stress. ASTM E1426-98, American Society for Testing and Materials, Philadelphia, PA.
31. Prevey, P.S. (1976) *Advances in X-Ray Analysis*, 19, 709.
32. Lu, J. (editor) (1996) Magnetic methods. *Handbook of Measurement of Residual Stresses*. Fairmont Press, Inc., Lilburn, GA.
33. Bate, S.K., Green, D., and Buttle, D. (1997) *A Review of Residual Stress Distributions in Welded Joints for the Defect Assessment of Offshore Structures*, HSE Books.
34. Fonseca, M.C., Teodosio, J.R., Rebello, J.M., and da Cruz, A.C. (2001) Residual stress state behaviour under fatigue loading in pipeline welded joints. *The Journal of Strain Analysis for Engineering Design*, 36(5), 465–472.
35. Kong, D.J., Zhou, C.Z., and Hu, A.P. (2011) Effect of laser shock on the mechanical properties of weld joint of X70 steel pipeline. *Journal of Jilin University (Engineering and Technology Edition)*, 41(5), 1507–1512.
36. Cammett, J.T., Prevey, P.S., and Jayaraman, N. (2005) The effect of shot peening coverage on residual stress, cold work and fatigue in a nickel-base superalloy. Proceedings of ICSP 9, Paris, France.
37. Cammett, J.T. and Prevey, P.S. (2001) Fatigue strength restoration in corrosion pitted 4340 alloy steel via low plasticity burnishing. Available at <http://www.lambdatechs.com/documents/228.pdf>. (last accessed December 2013).
38. Frost, N.E., Marsh, K.J., and Pook, L.P. (1974) *Metal Fatigue*, Clarendon Press, Oxford, p. 366.
39. Hornbach, D.J., Jayaraman, N., and Scheel, J.E. (2011) Engineered residual stress to mitigate stress corrosion cracking of stainless steel weldments. Available at <http://www.lambdatechs.com/documents/232.pdf>.
40. Chelette, D., Moore, P., Hornbach, D., Prevey, P., and Scheel, J. (2011) Mitigation of sulfide stress cracking in down hole P110 components via low plasticity burnishing. Advances in Materials for Oil & Gas Production, STG, Houston, TX.
41. Hornbach, D. and Scheel, J. (2012) Improving corrosion fatigue performance and damage tolerance of 410 stainless steel via LPB. Available at <http://www.lambdatechs.com/documents/285.pdf>. (last accessed 2013).
42. Hornbach, D.J. and Scheel, J.E. (2012) The effect of surface enhancement on improving the fatigue and sour service performance of downhole tubular components. ASME 2012 International Mechanical Engineering Congress and Exposition, Houston, TX.